

Interpretation of Polar Cap and Auroral  
Oval Equivalent Current Flow Using  
Inversion Techniques

G. Rostoker, D.W. Oldenburg & T.J. Hughes

FINAL REPORT

EPB  
Open File  
77-22

This document was produced  
by scanning the original publication.

Ce document est le produit d'une  
numérisation par balayage  
de la publication originale.



Energy, Mines and  
Resources Canada

Énergie, Mines et  
Ressources Canada

Earth Physics Branch

Direction de la physique du globe

---

1 Observatory Crescent  
Ottawa Canada  
K1A 0Y3

1 Place de l'Observatoire  
Ottawa Canada  
K1A 0Y3

GEOMAGNETIC SERVICE OF CANADA

Interpretation of Polar Cap and Auroral Oval Equivalent  
Current Flow Using Inversion Techniques

G. Rostoker, D.W. Oldenburg and T.J. Hughes

54 pp.  
Price \$10.00

Earth Physics Branch Open File No. 77-22  
Ottawa, Canada  
1977

NOT FOR REPRODUCTION

FINAL REPORT

Interpretation of Polar Cap and Auroral  
Oval Equivalent Current Flow Using  
Inversion Techniques

by

G. Rostoker, D. W. Oldenburg and T. J. Hughes

EMR Contract No.            OSQ 76-00019  
DSS File Number        15SQ 23235-6-0296

March 31, 1977

Earth Physics Branch Open File 77-22

## FINAL REPORT

### Interpretation of Polar Cap and Auroral Oval Equivalent Current Flow Using Inversion Techniques

---

EMR Contract No. OSQ 76-00019  
DSS File Number 15SQ 23235-6-0296

Principal Investigator  
(Contractor)

Dr. Gordon Rostoker  
Associate Professor of Physics  
University of Alberta

Co-Investigators

Dr. D. W. Oldenburg  
Mr. T. J. Hughes

#### Abstract

Ground based magnetometer data have been used extensively in the past to infer the pattern of equivalent current flow above the earth's surface. However it was not possible to assign real current flow characteristics to the ionosphere and magnetosphere until in situ mapping of field-aligned current flow penetrating the auroral oval was carried out. Enhanced knowledge of real current flow permits the use of more sophisticated techniques to quantitatively evaluate the behaviour of the auroral electrojets which are responsible for the major magnetic variations observed at the earth's surface. This report describes the development of inversion techniques which can be used to provide quantitative information on the strength and distribution of auroral electrojet currents in the evening sector. The model current systems used involve both the normal three dimensional current loop whose ionospheric portion is the east-west electrojet, and the north-south Pedersen ionospheric currents linked to the magnetosphere by east-west oriented field-aligned sheet currents. We demonstrate, in this report, the ability of this technique to detect multiple electrojet configurations in the evening sector auroral oval.

## Introduction

It is now generally accepted that the outer regions of the earth's magnetosphere are coupled to the ionosphere by field-aligned electric currents (Birkeland, 1908, 1913; Alfvén, 1939; Fejer, 1961; Kern, 1962; Boström, 1964). The magnetic effects of these currents have been detected above the auroral oval using polar orbiting satellites (Zmuda et al., 1967; Zmuda et al., 1970; Armstrong and Zmuda, 1970, 1974) and using ground based magnetometer arrays (Hughes and Rostoker, 1977).

Knowledge of the gross field-aligned current configuration derived in recent years by Sugiura and Potemra (1976) and Iijima and Potemra (1976) has allowed the development of models of the real magnetosphere-ionosphere current configuration (Yasuhara et al., 1975; Hughes and Rostoker, 1977) and studies of the relationships among the field-aligned currents and the ionospheric electrojets and auroral distribution (Armstrong et al., 1975; Wallis et al., 1976; Kamide et al., 1976) have tied together many of the important auroral parameters and accordingly improved our understanding of the basic auroral zone processes.

The development of coordinated ground based magnetometer arrays now presents the possibility of more effectively evaluating the level and character of auroral zone magnetic activity through the use of realistic current models and inversion techniques. The solution of the inverse problem involves the manipulation of a suite of ground based data to infer ionospheric and magnetospheric current systems in the framework of a specific current system model. The inverse problem has been formally solved by using linear inverse theory by Backus and Gilbert (1970) and

has been applied to the problem of upper atmospheric current flow by Oldenburg (1976). In this report we shall utilize linear inverse theory to provide estimates of current intensity and distribution across the auroral oval in the evening sector and in the hours immediately preceding local magnetic dusk. We shall show that the westward electrojet penetrates into the pre-midnight quadrant to the north of the eastward (steady state) convection electrojet, but that it is often absent in the region near the dusk meridian.

### Linear Inverse Theory

The magnetic field perturbations from the three-dimensional east-west system (Kisabeth and Rostoker, 1977) can be inverted to obtain estimates of the height-integrated ionospheric Hall current density (Oldenburg, 1976). Once the parameters defining the geometry of the current system (longitude of the eastern and western field-aligned current sheets, and the northern and southern latitudinal boundaries of the ionospheric current) have been specified, the magnetic field observations on the surface of the earth ( $r=a$ ), at colatitude  $\theta_0$ , and longitude  $\phi_0$  are obtained from

$$B_j^{EW}(a, \theta_0, \phi_0) = \int_{\theta_1}^{\theta_2} J_H(\theta) G_j^{EW}(a, \theta_0, \phi_0; \theta) d\theta \quad j=1,2,\dots,N \quad (1)$$

where  $B_j^{EW}$  is any component of the magnetic field,  $J_H(\theta)$  is the Hall current density in  $\text{Am}^{-1}$ , and  $\theta_1$  and  $\theta_2$  are the colatitude limits of the ionospheric current.  $G_j^{EW}$  is the Fréchet kernel or Green's function for the problem and is dependent upon the geometry of the current system

as well as the location on the earth's surface where the magnetic datum is obtained.

Kisabeth (1977) has used a derivation based on magnetic charge to show that the magnetic perturbations from the three-dimensional north-south current system can be computed in a manner similar to (1), namely,

$$B_j^{NS}(a, \theta_0, \phi_0) = \int_{\theta_1}^{\theta_2} J_p(\theta) G_j^{NS}(a, \theta_0, \phi_0; \theta) d\theta \quad j=1,2,\dots,N \quad (2)$$

where  $J_p(\theta)$  is the Pederson current density.

Since both of these systems exist simultaneously the ground-based magnetic observations are

$$B_j = B_j^{EW} + B_j^{NS} \quad j = 1, \dots, N \quad (3)$$

Assuming that the electric field is purely north-south,

$$J_p(\theta) = \frac{\sigma_p}{\sigma_H} J_H(\theta) \quad (4)$$

where  $\sigma_H$  and  $\sigma_p$  are respectively the Hall and Pedersen conductivities.

Equations (1) and (2) can be combined to give

$$\begin{aligned} B_j(a, \theta_0, \phi_0) &= \int_{\theta_1}^{\theta_2} J_H(\theta) \left( G_j^{EW}(a, \theta_0, \phi_0; \theta) + \frac{\sigma_p}{\sigma_H} G_j^{NS}(a, \theta_0, \phi_0; \theta) \right) d\theta \\ &\equiv \int_{\theta_1}^{\theta_2} J(\theta) G_j(a, \theta_0, \phi_0; \theta) d\theta \end{aligned} \quad (5)$$

where  $G_j = G_j^{EW} + \frac{\sigma_p}{\sigma_H} G_j^{NS}$  is the complete Fréchet kernel for the problem, and for convenience we have dropped the subscript H on  $J_H(\theta)$ . This formulation therefore requires that the ratio  $\sigma_p/\sigma_H$  be known; if it is not, this ratio may be regarded as a free parameter which we can feel free to adjust until the discrepancies between the observations and model calculations are minimized.

The inverse problem which we shall solve poses the following question: given the N magnetic measurements  $B_j$  what can be said about the current density  $J(\theta)$  in the region  $\theta_1 \leq \theta_0 \leq \theta_2$ . Linear inverse theory shows that the only estimates available to us are linear combinations of the data themselves, that is,

$$\langle J(\theta_0) \rangle = \sum_{j=1}^N a_j(\theta_0) B_j = \int_{\theta_1}^{\theta_2} J(\theta) A(\theta, \theta_0) d\theta \quad (6)$$

where

$$A(\theta, \theta_0) = \sum_{j=1}^N a_j(\theta_0) G_j(\theta) . \quad (7)$$

$A(\theta, \theta_0)$  is called the averaging function and is effectively the window through which the current density structure is viewed.

The  $a_j$ 's in equation (7) can be computed in a variety of ways. The method employed here is the quadratic criterion of Backus and Gilbert (1970) because this leads to averaging functions which are not contaminated by sidelobes (Oldenburg, 1977). If  $A(\theta, \theta_0)$  is narrow and peaked at  $\theta = \theta_0$  then  $\langle J(\theta_0) \rangle$  will be a localized estimate of the current density in a region near  $\theta = \theta_0$ . Importantly, this formulation also solves the non-uniqueness problem, *for all possible current densities,  $J(\theta)$ , which*

give rise to the observations provide the same estimate  $\langle J(\theta_0) \rangle$  when they are averaged with  $A(\theta, \theta_0)$ . Also, the observational errors (or errors incurred by a departure of the current system from the model assumed here) may be included in the analysis to provide estimates of the standard deviation,  $\sigma(\theta_0)$ , of  $\langle J(\theta_0) \rangle$ . Our final knowledge about the current density at  $\theta = \theta_0$  is therefore codified by the three quantities:  $\langle J(\theta_0) \rangle$ ,  $\sigma(\theta_0)$ , and  $A(\theta, \theta_0)$ .

In addition to the unique estimates of the current density it is also possible to obtain estimates of the total current flowing in the system. To complete this calculation it is desired to find a linear combination of Fréchet kernels to make a constant function in the region  $\theta_1 \leq \theta \leq \theta_2$ . Oldenburg (1976) has shown that those estimates are relatively insensitive to errors in the data and are therefore well-determined.

Lastly, it must be emphasized that although there exists infinitely many current densities which will recreate the observations, the averages,  $\langle J(\theta) \rangle$ , will not do so. Interpretation might be facilitated by examining some explicit current densities which reproduce the observations. Such current densities may be found by minimizing a specific functional subject to the constraints that the observations are reproduced. The additional constraint that the current density be zero at the northern and southern limits of the electrojet may also be included if desired. The functionals which lead to sets of linear equations are:

$$\phi_1 = \int_{\theta_1}^{\theta_2} [J(\theta)]^2 d\theta \quad (8)$$

and

$$\phi_2 = \int_{\theta_1}^{\theta_2} [J^1(\theta)]^2 d\theta \quad (9)$$

where  $J^1(\theta) = \frac{dJ(\theta)}{d\theta}$

The current densities minimizing (8) and (9) (subject to the constraints) are respectively the "smallest" and "flattest" models. To ensure that

$$J(\theta_1) = J(\theta_2) = 0 \tag{10}$$

it is computationally expedient to minimize

$$\phi_1 = \int_{\theta_1}^{\theta_2} [f(\theta) J(\theta)]^2 d\theta \tag{11}$$

where  $f(\theta)$  is a function which is equal to 1.0 everywhere except near  $\theta_1$  and  $\theta_2$  where it rises to some large amplitude. The minimization of (11) subject to the constraints (5) shows that

$$J(\theta) = \frac{1}{[f(\theta)]^2} \sum_{j=1}^N a_j G_j(\theta) \tag{12}$$

where the  $a_j$ 's are the solution to the  $N \times N$  system of equations

$$B_j = \sum_{i=1}^N a_i r_{ij} \quad j = 1, \dots, N \tag{13}$$

and

$$r_{ij} = \int_{\theta_1}^{\theta_2} [f(\theta)]^2 G_i(\theta) G_j(\theta) d\theta \tag{14}$$

To find the flattest model we define

$$H_j(\theta) = \int_{\theta_1}^{\theta} G_j(u) du \tag{15}$$

The minimization of (9) subject to the constraints (5) and (10) readily leads to the conclusion that

$$J^1(\theta) = n - \sum_{j=1}^N a_j H_j(\theta) \quad (16)$$

where

$$n = \frac{1}{\theta_2 - \theta_1} \sum_j a_j \int_{\theta_1}^{\theta_2} H_j(\theta) d\theta \quad (17)$$

The system of equations to be solved is

$$B_j = n \int_{\theta_1}^{\theta_2} H_j(\theta) d\theta + \sum_i a_i R_{ij} \quad j=1,2,\dots,N \quad (18)$$

where

$$R_{ij} = \int_{\theta_1}^{\theta_2} H_i(\theta) H_j(\theta) d\theta$$

The current density  $J(\theta)$  is then readily recovered from equation (16).

### Discussion of the Theory

In order to demonstrate the application of linear inverse theory in the determination of latitudinal current distributions from ground based magnetic data, a latitude profile of magnetic data was synthesized from a known model three dimensional current system. The model used was that for a three dimensional east-west uniform current distribution of strength 2.21 A/m (Kisabeth and Rostoker, 1977) with the current limited to 4° of latitude (66° to 70°) and 20° of longitude. Five values of the north-south (X) and vertical (Z) magnetic field perturbations were generated (Figure 1). These data were then used as input to the inversion computer code, subject to different model parameters.

In the first example, the current was constrained to lie between 20° and 24° colatitude, the same limits used in the generation of the data. Figure 2 shows the result of the current inversion. The solid line is a plot of the estimates  $\langle J(\theta) \rangle$  from the inversion, and the broken line is derived for the flattest model. In this case, the estimates agree with the real values, because of the uniformity of the real current distribution, and because all parameters (length, width, position, etc.) were specified to be exactly correct. The flattest model has been clamped at the ends (viz. the current has been constrained to be zero outside the latitudinal limits read off the latitude profile) (see Eq. 16), and because we have constrained the current to lie between 20° and 24° colatitude, the model current density oscillates spatially in order to fit the observations as well as to satisfy the minimization of

$$\phi = \int_{\theta_1}^{\theta_2} [J^1(\theta)]^2 d\theta$$

Figure 1: North-south (X) and vertical components of magnetic field perturbations due to three dimensional westward current system. The uniform current distribution strength 2.21 A/m was centered between 66°N and 70°N.

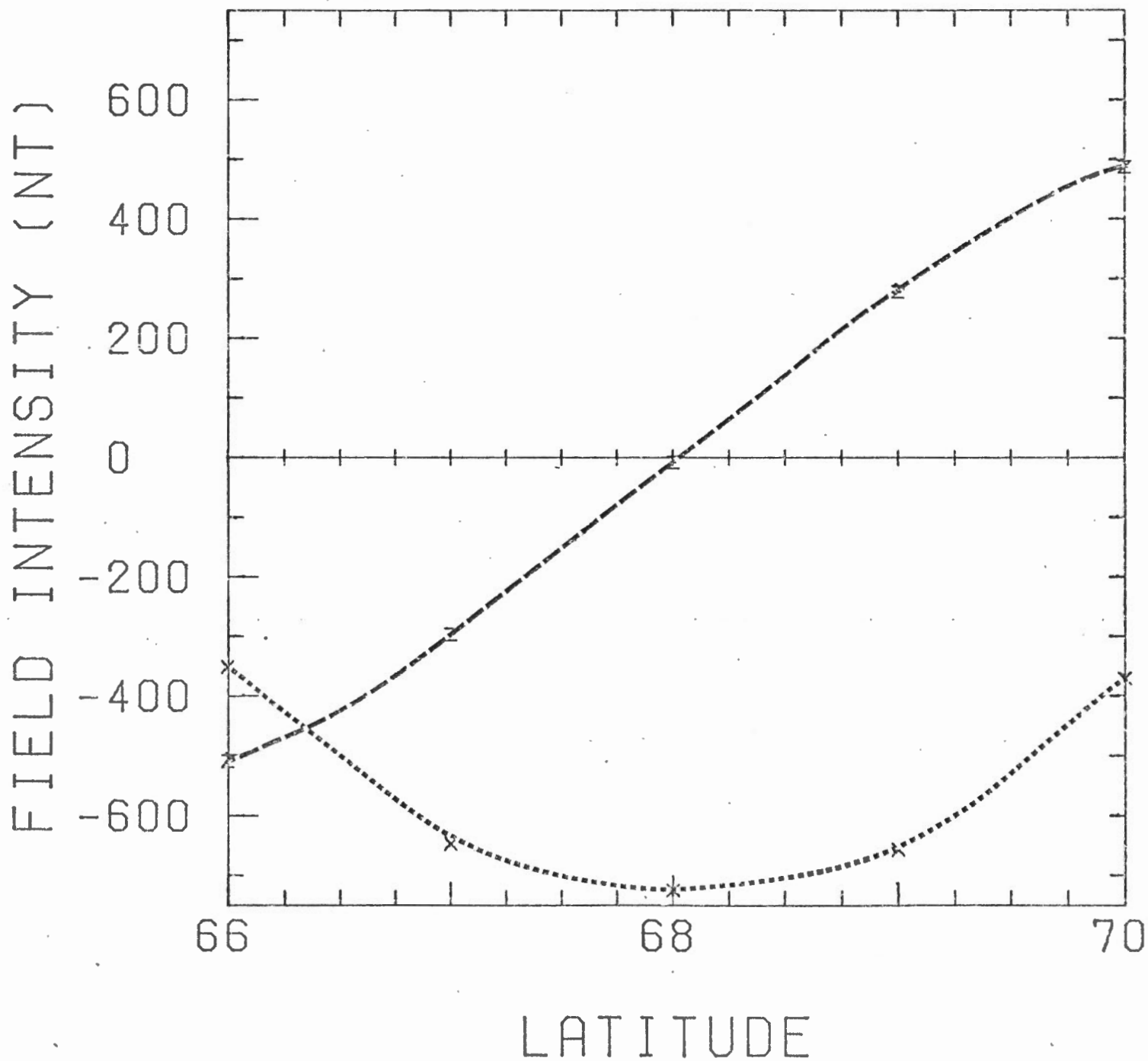
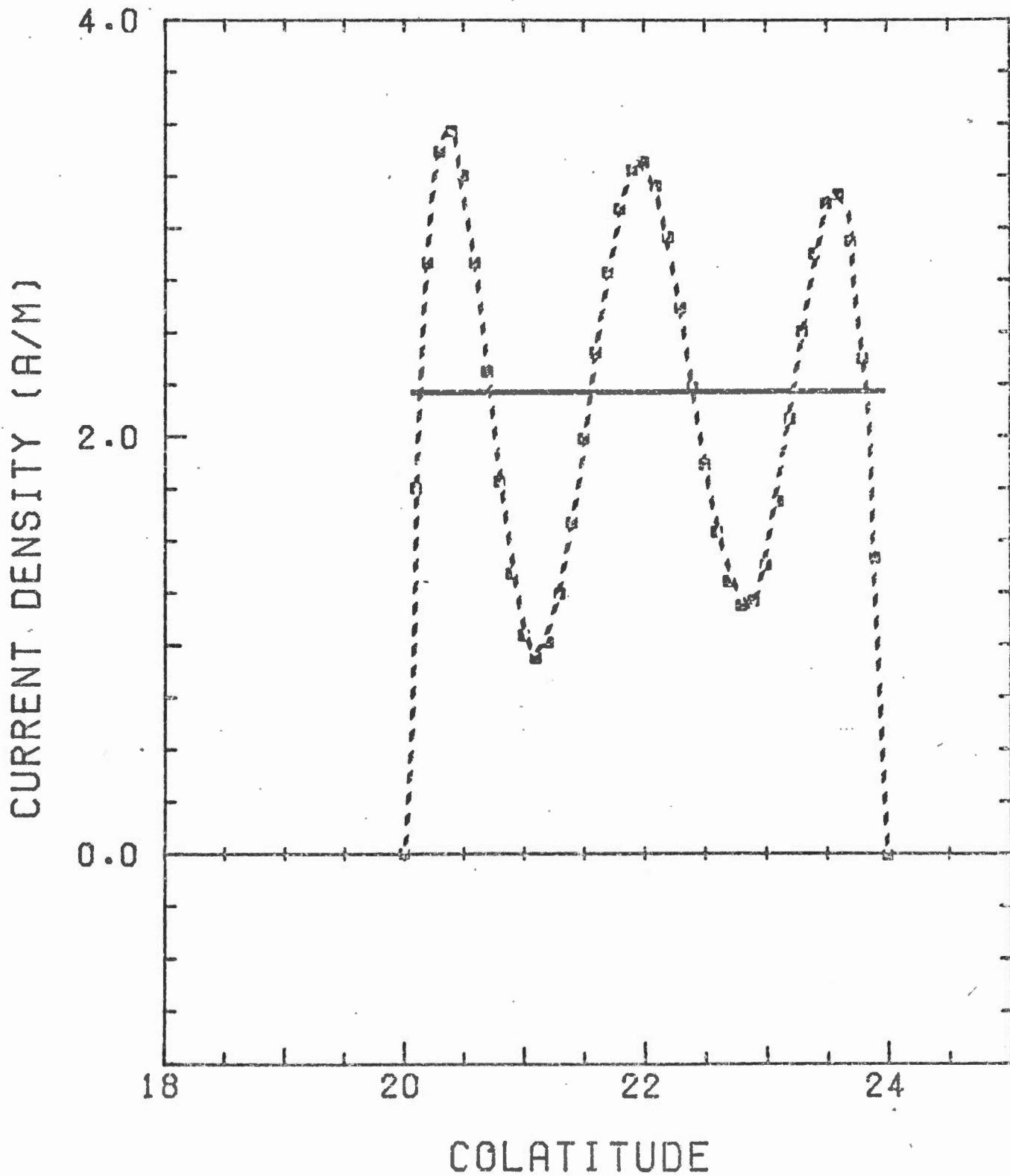


Figure 2: Results of inversion of the data in Figure 1, for the case of fixing the current limits to  $20^\circ$  and  $24^\circ$  colatitude. (---) - plot of the current densities derived in the flattest model. (—) - a plot of the current density estimates  $\langle J(\theta) \rangle$ . Westward flowing current is positive in this plot and subsequent plots of current density. Note that the horizontal axis is colatitude.



The second example (Fig. 3) shows the results of relaxing the current boundary constraint. That is, Figure 3 is the result of inverting the same data as used in Figure 2, but this time restricting the inverted current to be between  $19.5^\circ$  and  $24.5^\circ$  colatitude. In this case,  $\langle J(\theta) \rangle$  is no longer the boxcar function as in the first example, but has rounded edges. (The actual current distribution has also been plotted in Figure 3, as a dashed line.) Outside the limits shown, the computer program in effect attempts to reduce the value of  $\langle J(\theta) \rangle$  in accordance with the fact that there is really no current outside these limits. The broken line is the flattest model which fits the data. Since, in this case, we do not force the current to be clamped at the real current boundaries, this model is a fair approximation to the real current.

Another example is shown in Figure 4. In this case all the current model parameters were set to the values used in generating the data, but the magnetic perturbations from the field aligned currents and the ring current were omitted from the calculations in the inverse problem. In this case,  $\langle J(\theta) \rangle$  is reduced, consistent with the fact that the field aligned currents produce  $-\Delta H$  in the eastward electrojet regime which, in part, cancels the  $+\Delta H$  produced by the ionospheric electrojet. The result of this change is that the flattest model exhibits large amplitude spatial oscillations, indicating an incorrect model has been used.

A final theoretical example is provided by relaxing the latitudinal extent constraint as well as including only the ionospheric current in the model (Figure 5). Although Figs. 4 and 5 differ quantitatively, the qualitative nature of the two is very similar. Both give a highly oscillatory current density for the flattest model, again indicating an incorrect choice of model.

Figure 3: Same as Figure 2 but for the case of broad current limits (19.5° and 24.5° colatitude). The dashed line (---) is a plot of the actual current density used to generate the data of Figure 1.

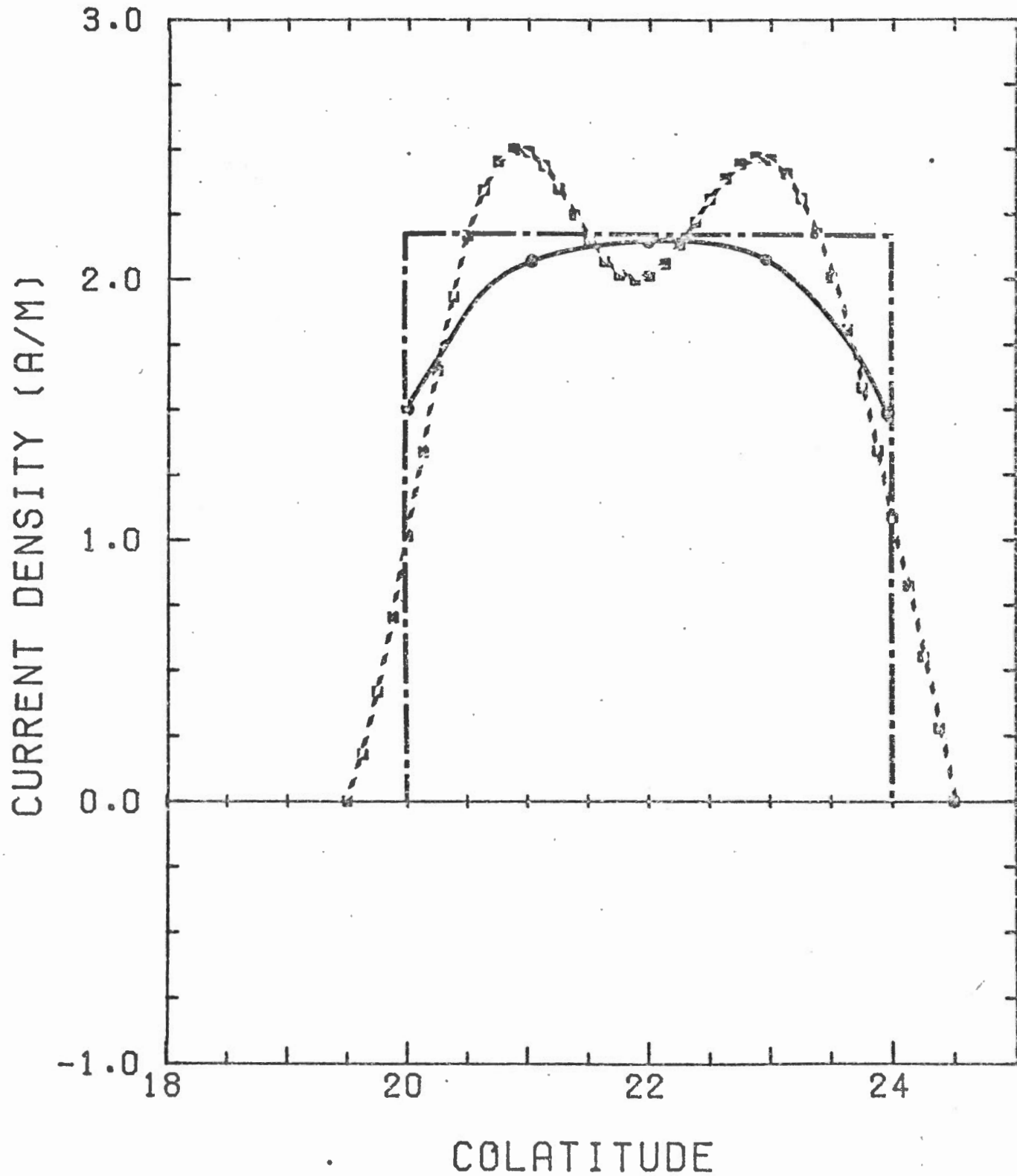


Figure 4: Same as Figure 2 but in this case only the ionospheric current contribution was used in the inversion calculations.

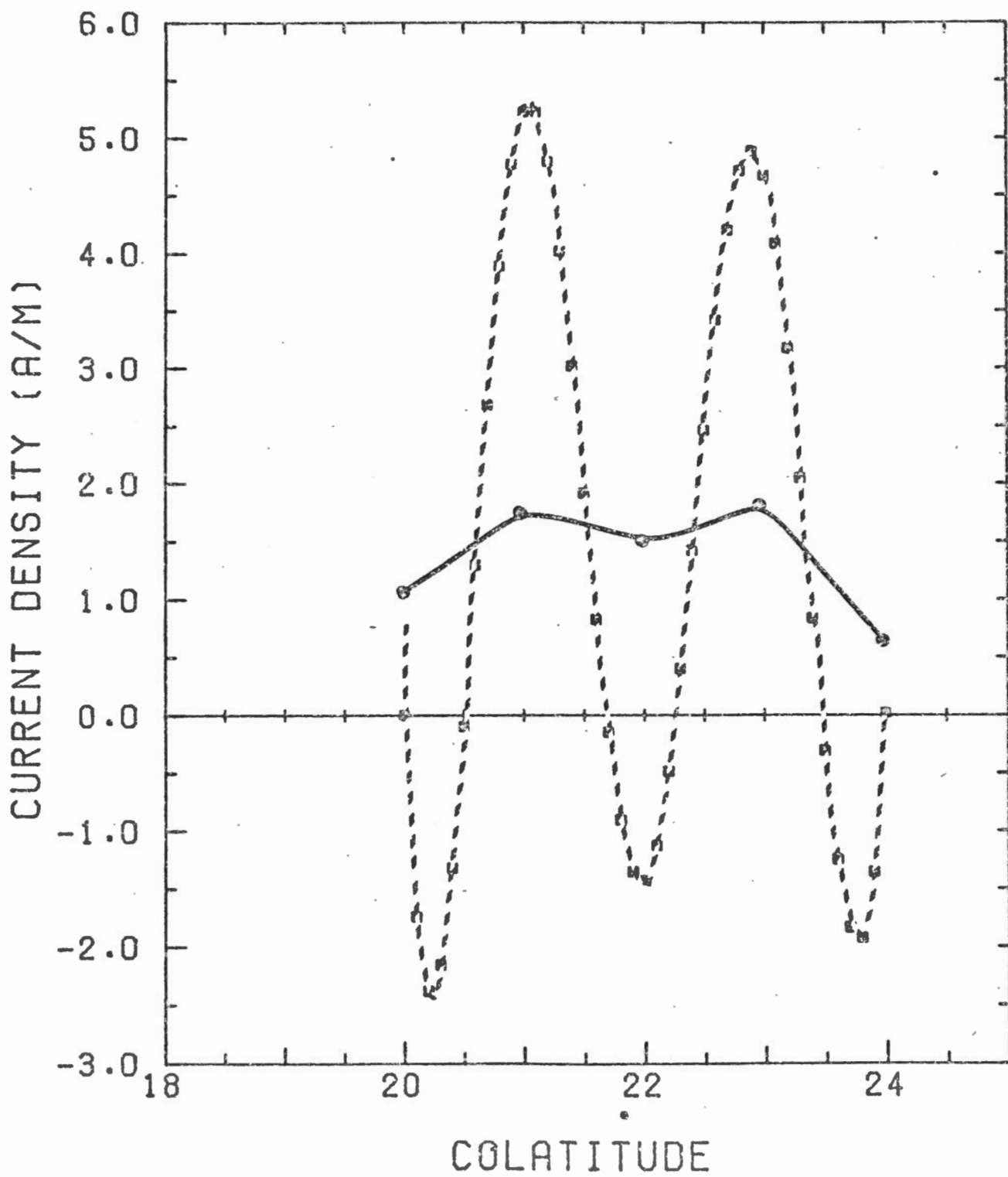
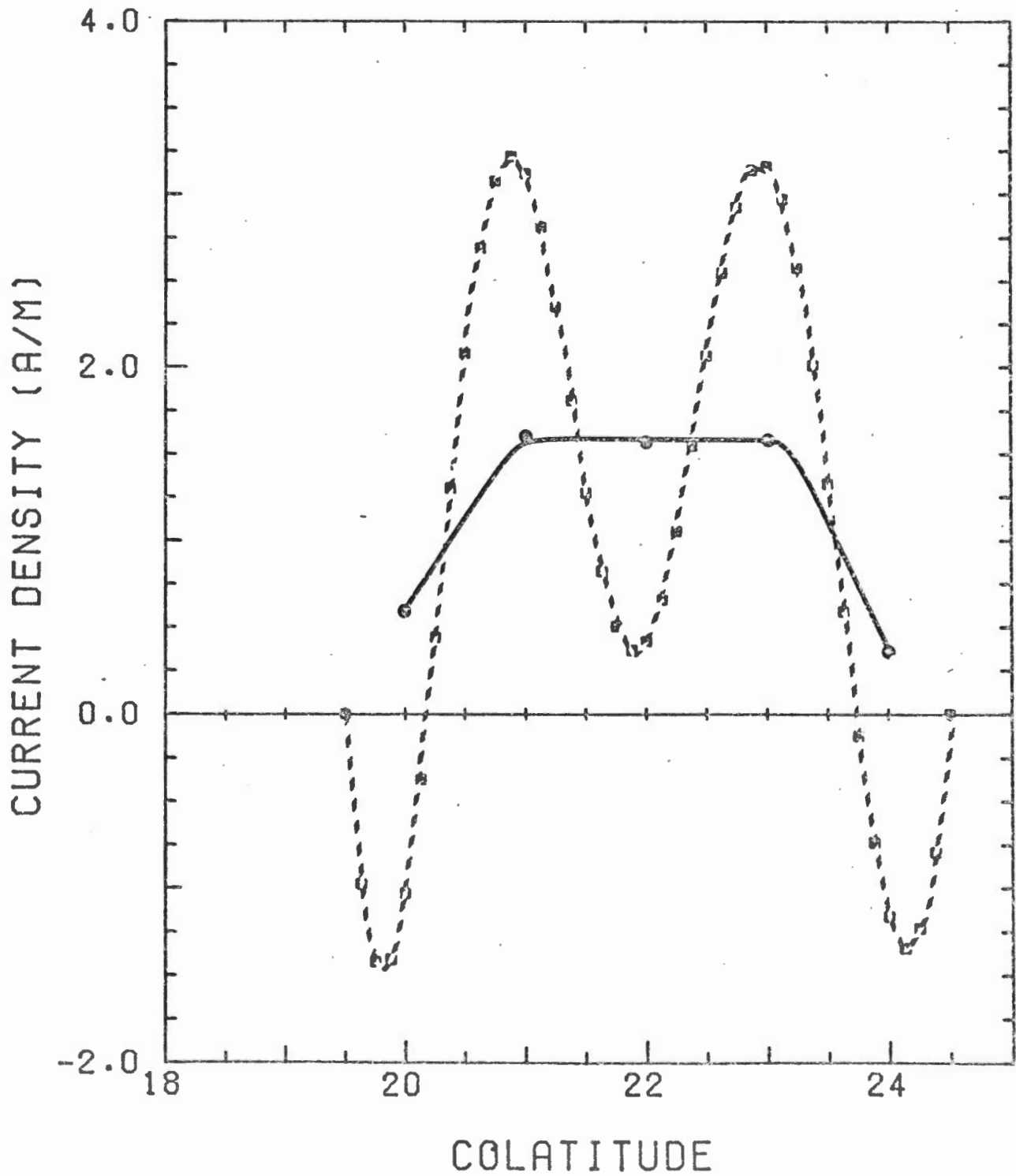


Figure 5: Same as Figure 3 (i.e. broad current limits) but in this case only the ionospheric current contribution was used in the inversion calculations.



The observations described above serve to demonstrate several features of the inverse problem. First, all the above flattest models of current distribution ( $J_F(\theta)$ ) if used in the forward problem (i.e. if we calculate  $\Delta H$  and  $\Delta Z$  using  $J_F$  as the current distribution) will produce values of  $\Delta H$  and  $\Delta Z$  that agree with the observations within the constraints of the problem. (Figures 6, 7, 8 and 9 are plots of the original data  $(X, Z)$  and the computed results  $(\square, \Delta)$  for the four theoretical cases described above.) However, each of these models are different, and this fact emphasizes the fundamental problem of inversion techniques, that of the non-uniqueness of the result. Here we have four different models of current density (and indeed geometry) each capable of reproducing the observations. As discussed in the theory section, the only unique calculation that can be made is that of  $\langle J(\theta) \rangle$ .  $\langle J(\theta) \rangle$  is however dependent upon the Fréchet kernels,  $G_j$  (equation 1), and is therefore model dependent. This is apparent from the different nature of the  $\langle J(\theta) \rangle$  curves for each of the theoretical cases, but for a given model and data set  $\langle J(\theta) \rangle$  is unique.

Before proceeding to the data, a brief discussion of the philosophy of the approach to the modeling problem should be made. As seen in the theoretical results, choice of an incorrect model, or incorrect model parameters, leads to spatially oscillatory current density for the flattest models. (The same is true of the "smallest" model; indeed the smallest model is very sensitive to errors.) However, if a set of magnetic field values were given, and it was desired to find a model that fit the data, and suppose that one current boundary was chosen incorrectly, then the result would be similar to that shown in Figure 10. The current density for the flattest model is spatially oscillatory, and the current density

Figure 6: X( $\square$ ) and Z( $\triangle$ ) perturbations calculated using the flattest model of current density in which the current was confined between  $20^\circ$  and  $24^\circ$  colatitude. The symbols X and Z are the same values as in Figure 1.

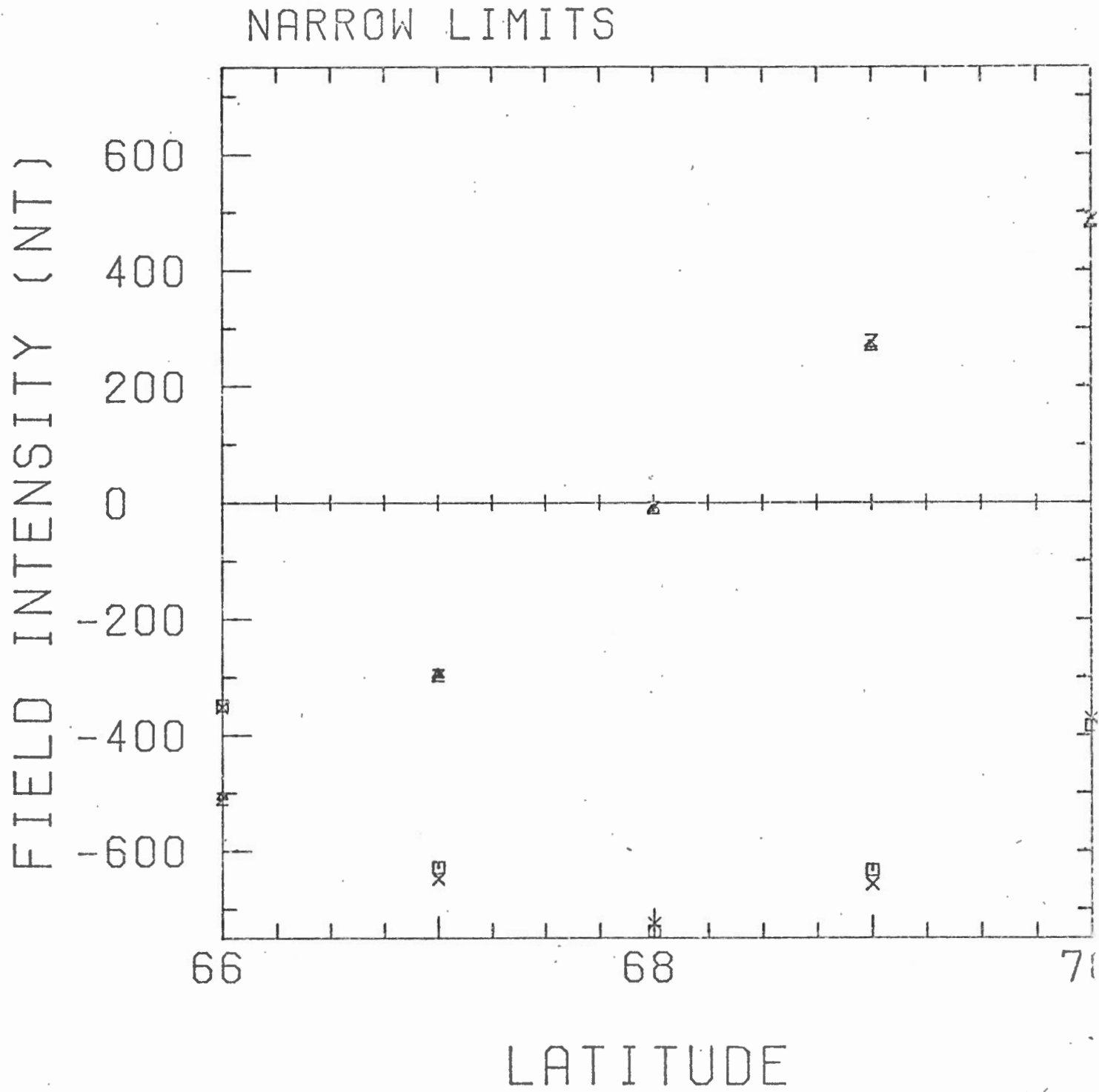


Figure 7: Same as Figure 6 but for the case of the broad current limits.

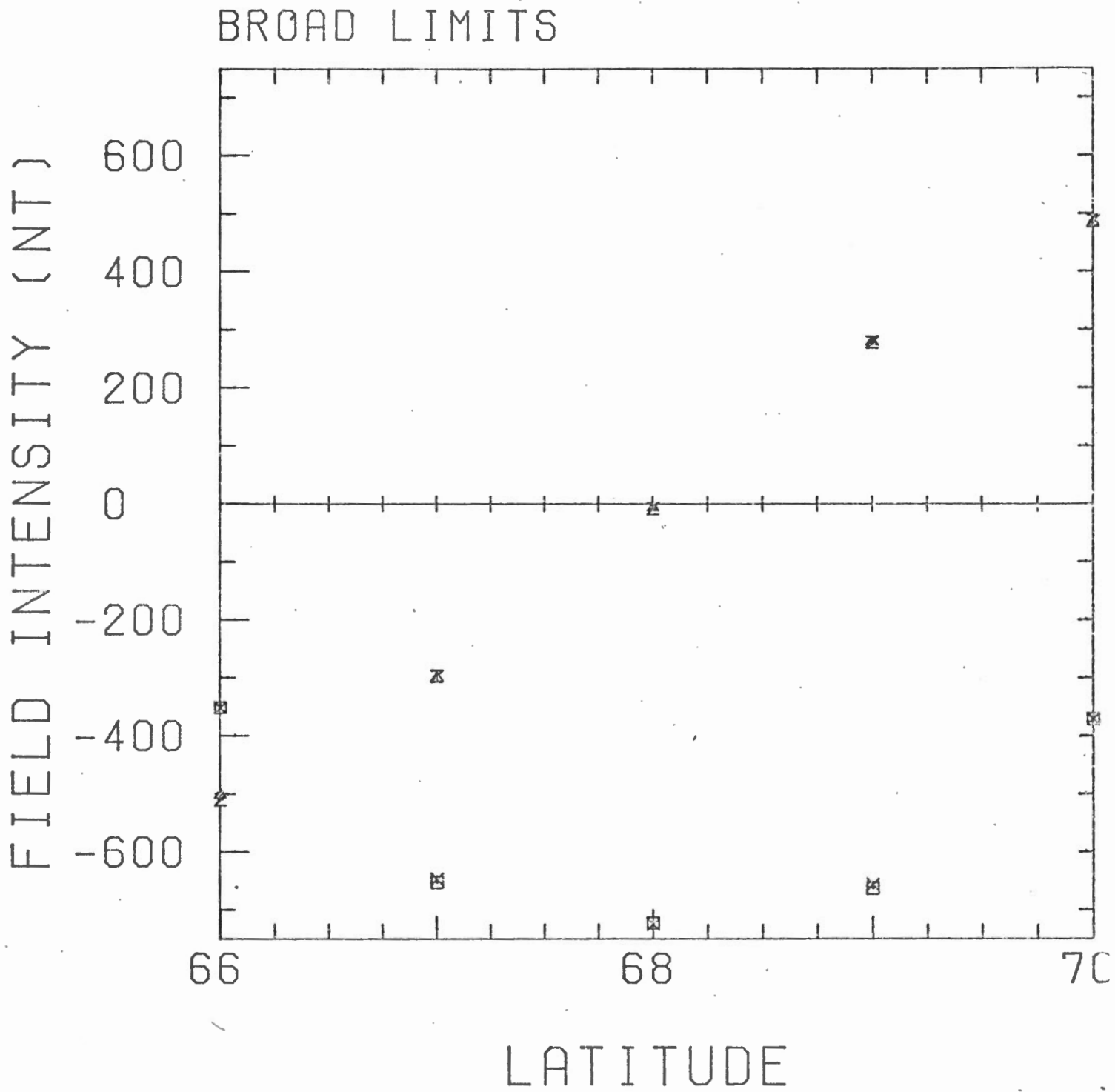


Figure 8: Same as Figure 6 but for the flattest model plotted in Figure 4.

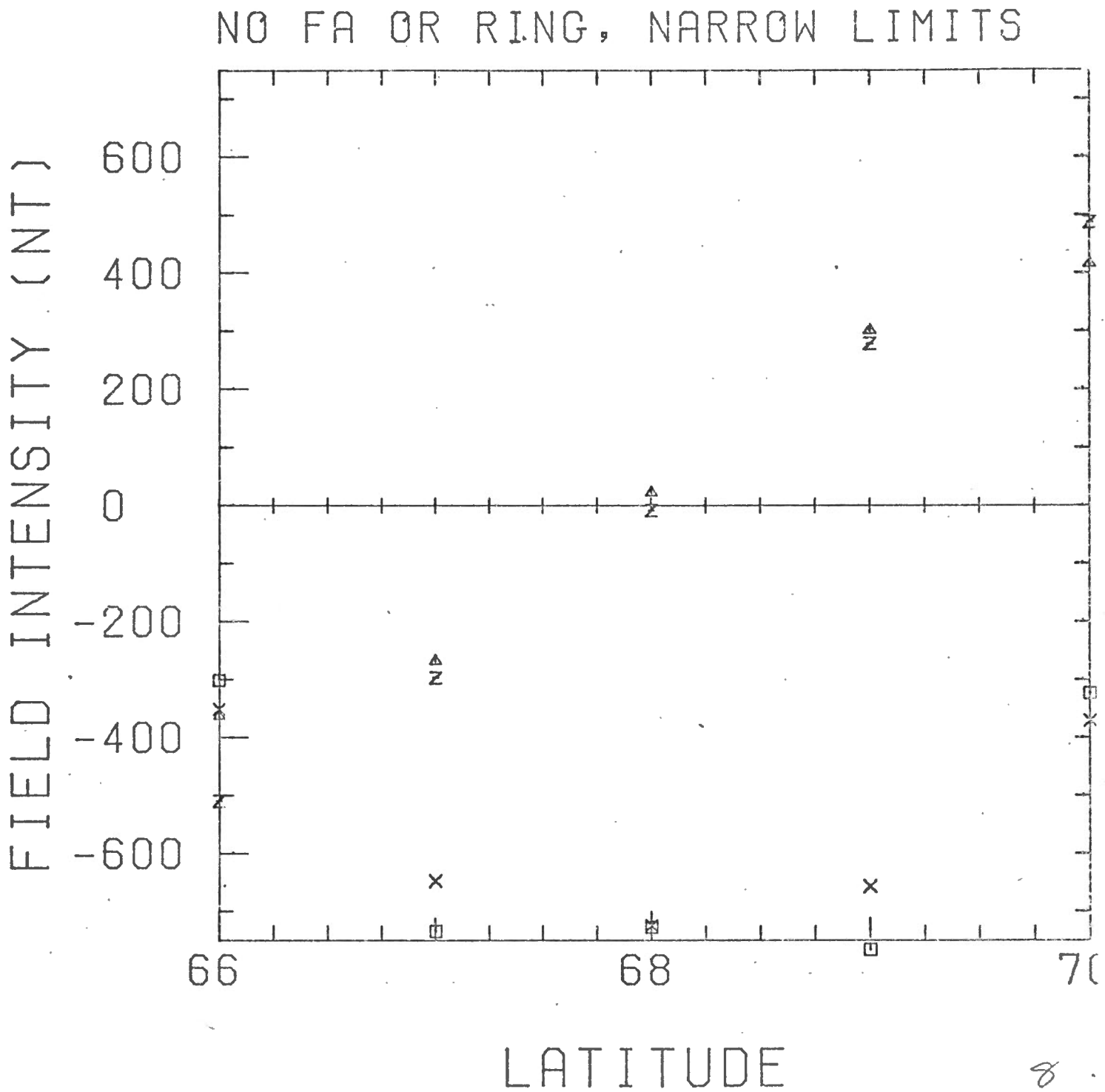


Figure 9: Same as Figure 6 but for the flattest model plotted in Figure 5.

NO FA OR RING, BROAD LIMITS

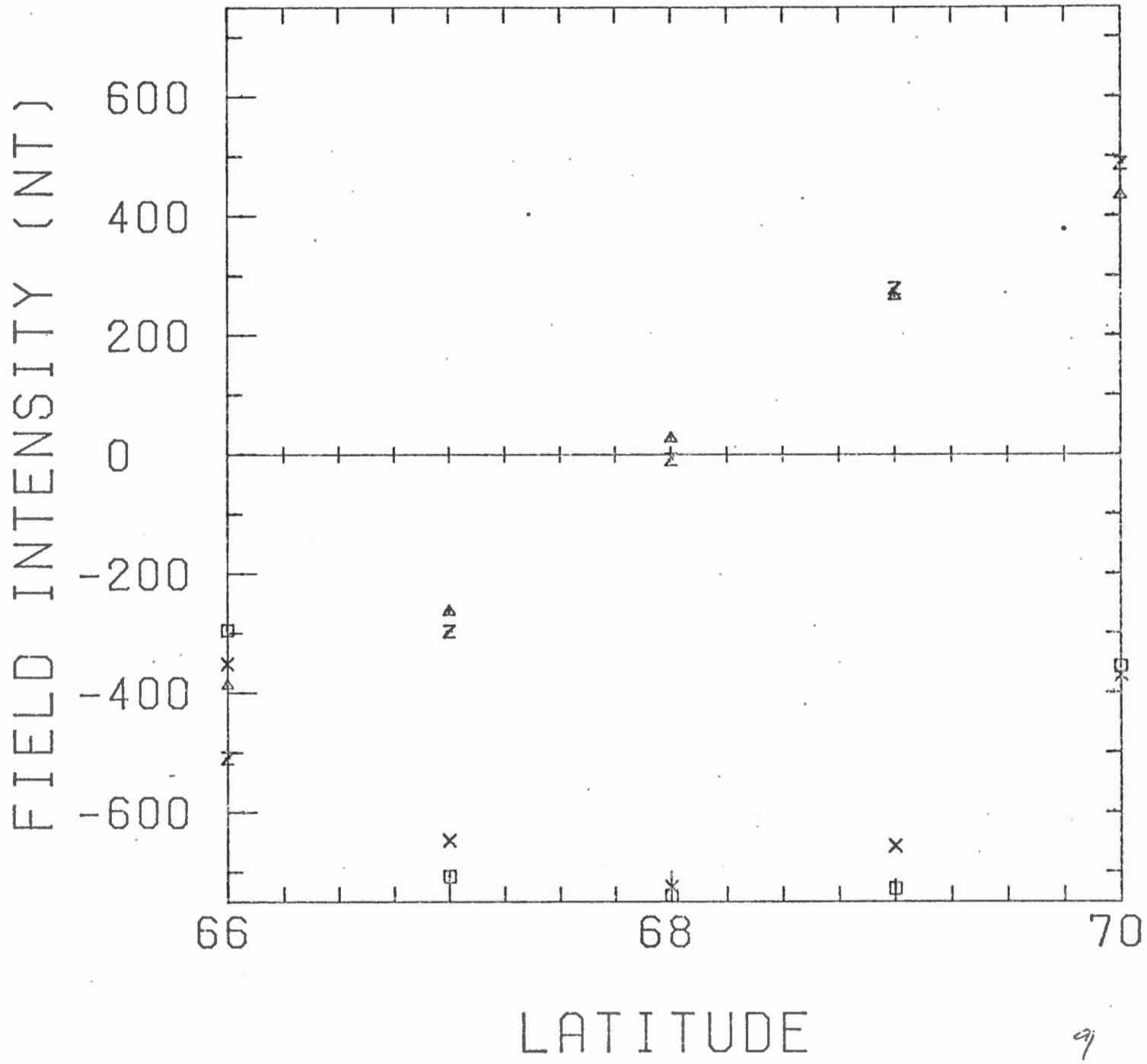
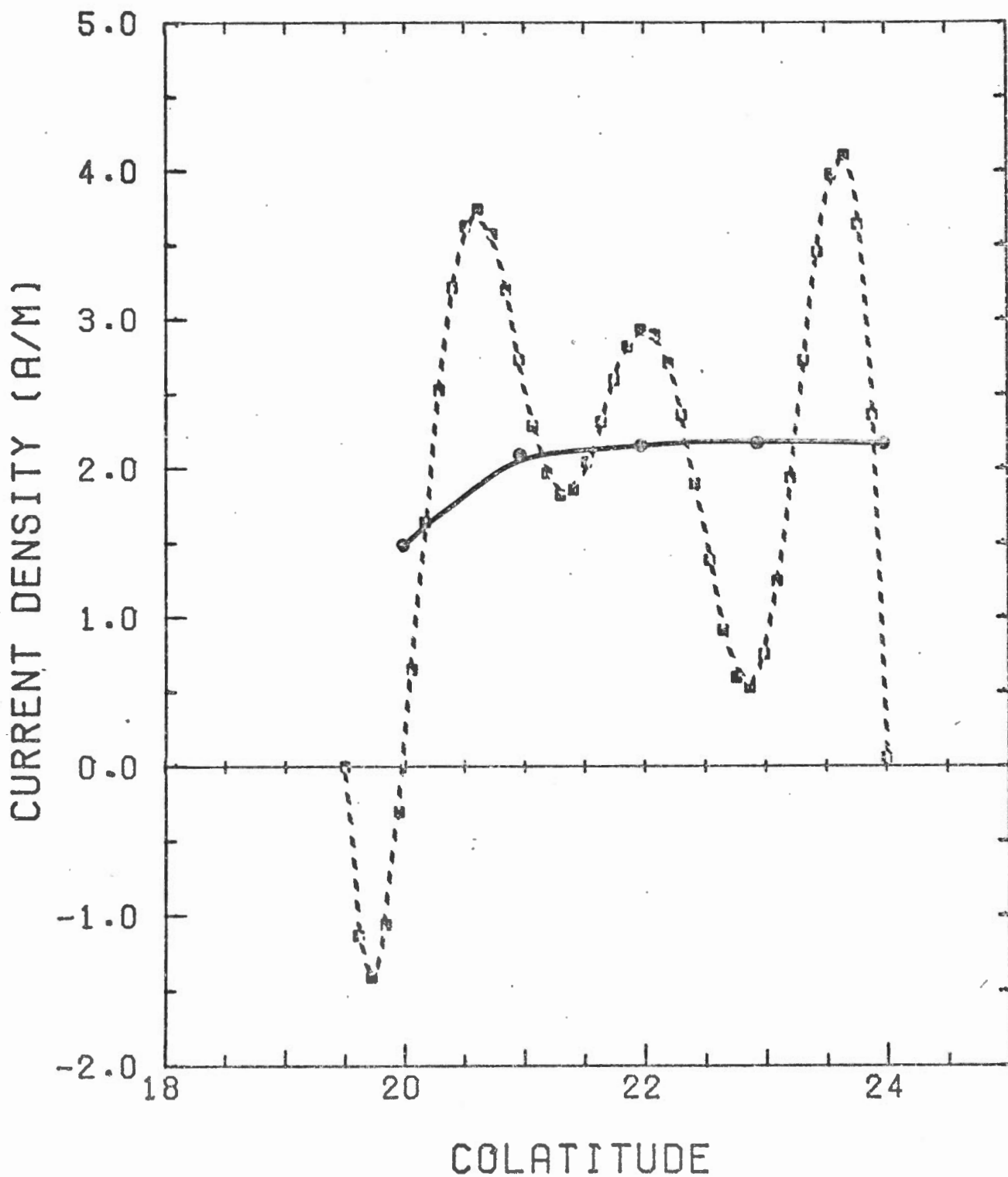


Figure 10: Results of inversion of the data plotted in Figure 1, but with the current boundaries set to  $19.5^\circ$  and  $24^\circ$  colatitude. (---): the flattest model current densities. (—): the estimates  $\langle J(\theta) \rangle$ .



estimator curve deviates from the known current density at the poleward boundary. The fit to the data in this example is very good, with a root mean square relative error of less than 1%. Given no a priori knowledge of the nature of the current distribution, this result might be quite acceptable. However, during episodes of strong magnetospheric activity ionospheric conductivity and electric fields may become quite intense in spatially localized regions. For such cases, one might not expect a smooth current distribution across the latitudinal extent of the auroral oval and hence use of the flattest model might not be justified. However, in our study we have dealt only with the modelling of data obtained from hourly averages of the magnetic field perturbations. Since substorm electrojet elements have a lifetime of  $\sim 15-30$  minutes insofar as the time scale of the intense auroral variations are concerned, our profiles then smear out the effects of intense localized electrojet elements. For this reason we decided to concentrate on the flattest models of current distribution, as they would be expected to best describe the large time scale current configurations which our latitude profiles depict.

#### Analysis of the Data

The primary data suite for this study is from the University of Alberta magnetometer line over a period of operation from day 332 of 1971 to day 24 of 1972. The meridian line lies along  $\sim 300^\circ\text{E}$  geomagnetic, and LMT is UT minus 8 hours (i.e. 0000 LMT = 0800 UT). The time period of interest in this report is from 2300 UT to 0700 UT (approximately 1500 MLT to 2300 MLT). Each station in the line is equipped with a three component fluxgate magnetometer and digital recording system. Measurements by the

system are accurate to  $\pm 1$  nT over a range of 1000 nT, and timing is considered accurate to  $\pm 0.1$  s, except at Contwoyto Lake where the accuracy is  $\pm 1$  min. The coordinates of the 8 digital observatories used in this study are given in Table 1. In addition, two observatories (Resolute Bay,  $83.0^{\circ}\text{N}$  and Newport,  $55.1^{\circ}\text{N}$ ) are operated on the  $300^{\circ}\text{E}$  meridian by other agencies and their data were used in this study to supplement the meridian line data.

For use in this study, the data were manipulated to produce hourly averaged values (centered on the half hour) of each component at each station, and latitude profiles were constructed for each hourly interval of interest. The horizontal components (H and D) were rotated so that the perturbation components of the field are presented in the geomagnetic (centered dipole) system.

In order to invert such data for the latitudinal current distribution, a model is required from which the magnetic field perturbations may be computed. As described in the theory section, the model is due to Kisabeth, and consists of both east-west and north-south current sheets, bounded by field-aligned currents, with closure in the magnetosphere. However, this model alone cannot account completely for the observed averaged magnetic perturbations for the magnetic local time sector from 1500 to 2300. Hughes and Rostoker (1977) have examined the data suite used in this present study, for all magnetic local times, and have found that there is an unbalanced upward field-aligned current flow in the poleward part of the auroral oval from about 1800 MLT to 2300 MLT. For the purposes of modelling, this current is a perturbation upon the simple east-west plus north-south current model. In light of the discussion of the theoretical models, it is apparent that

Table 1

## Coordinates and L Values of Magnetometer Line Sites

Site	Code Name	Geographic		Geomagnetic		L R <sub>E</sub>
		Latitude (°N)	Longitude (°E)	Latitude (°N)	Longitude (°E)	
Cambridge Bay	CAMB	69.1	255.0	76.8	296.6	19.5
Contwoyto Lake	CONT	65.5	249.7	72.6	295.8	11.3
Fort Reliance	RELI	62.7	251.0	70.3	300.1	8.9
Fort Smith	SMIT	60.0	248.0	67.3	300.0	6.8
Fort Chipewyan	FTCH	58.8	248.0	66.3	303.1	6.2
Fort McMurray	MCMU	56.7	248.8	64.2	303.5	5.4
Meanook	MENK	54.6	246.7	61.9	300.8	4.5
Leduc	LEDU	53.3	246.5	60.6	302.9	4.2

such a perturbation will affect the inversion results. The main effect of these net field-aligned currents appears in the D (east-west) component, and since  $\Delta D$  is most subject to other effects, such as surges, the D component has not been used in this study. As well, a global, average current model has been devised (Hughes and Rostoker, 1977) and the calculated magnetic field perturbations from this model, for the currents situated between 0200 MLT to 1200 MLT have been removed from the data. This has been done to ensure that the magnetic field data used in the inversion was due, as closely as could be determined, to current flow in the near vicinity of the meridian line.

Regarding the superposition of an east-west current system and a north-south current system, Mozer and Lucht (1974) have shown that for the local time sector 1500 to 2300, the average auroral zone electric field is almost purely northward, thus driving a northward Pedersen current and an eastward Hall current. Brekke et al. (1974) have shown that for quiet times, the ratio of the height integrated Hall to height integrated Pedersen conductivities is  $\sim 2$ , for all local times. These observations combine to yield an approximately constant north-south to east-west current density ratio of  $\sim 2$  for 1500 MLT to 2300 MLT. Trial inversions using Hall to Pedersen height integrated conductivity ratios of from 5.0 to 0.2 yielded best fitting models at a ratio of 2., and this value was used throughout this study.

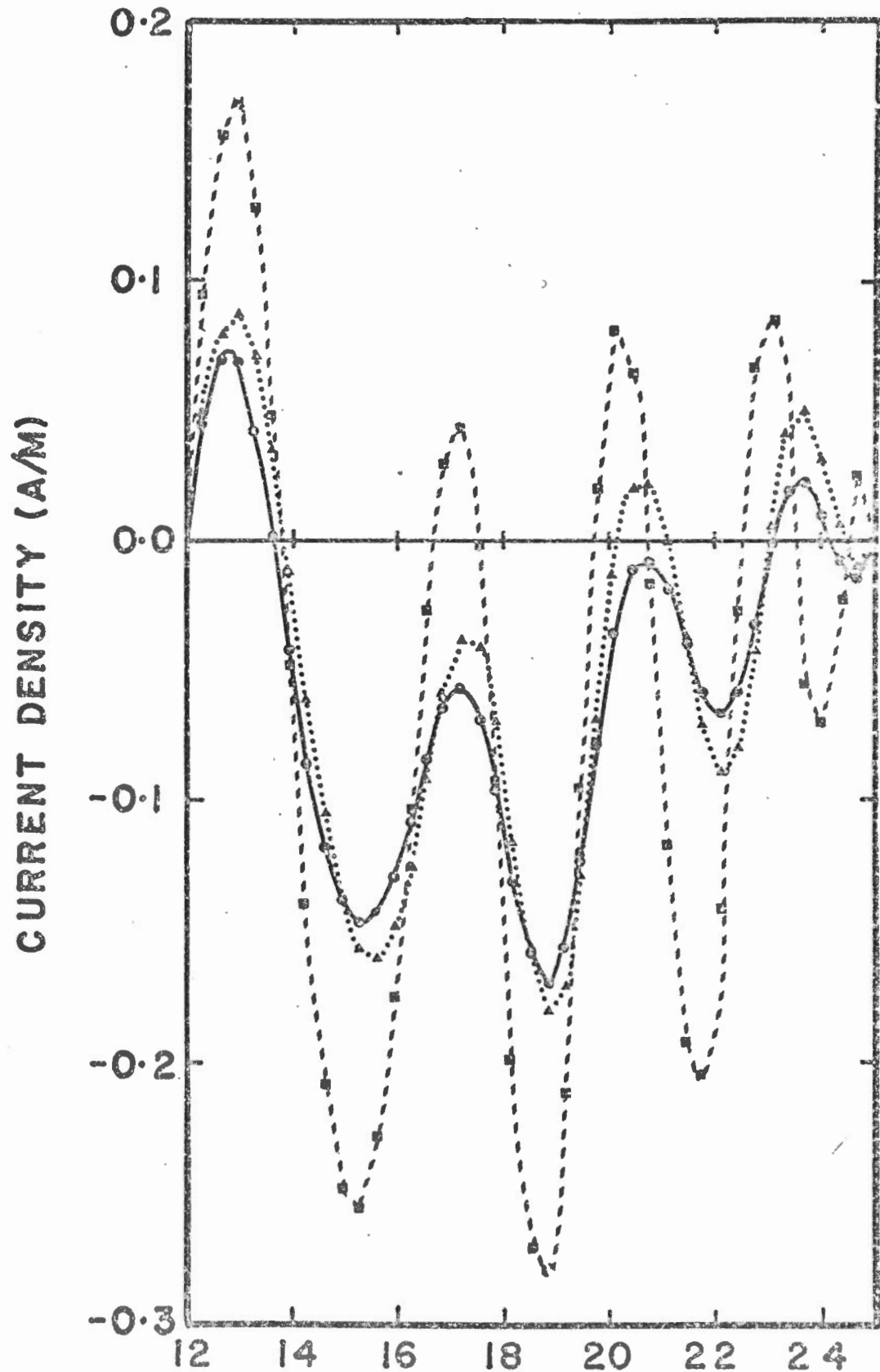
The north-south extent of the currents were determined to a first approximation from the  $\Delta Z$  extrema (Rostoker 1972) and expanded about  $1.5 - 2^\circ$  beyond this, and the east-west extrema were assumed to be local magnetic noon and 2200 MLT, as shown in the model of Hughes and Rostoker (1977).

Finally, before proceeding to the results of the data analysis, the effects of the assumed external current systems as well as the effect of the north-south current system upon inversions of real data should be examined. Figure 11a is a plot of three different flattest models, all for real data from day 3, 1972, 2300-2400 UT (1500-1600 MLT) [see Fig. 11b for the relevant latitude profile]. The broken line is the flattest model for the raw average data, using only an east-west current model. It is highly oscillatory, and the oscillations are of large amplitude, reminiscent of those theoretical models in which various incorrect current model parameters were used for the inversion. At this point, one must decide if the real current does oscillate in this manner or if rather the real current is smoother in character. As described above, it is inferred from this curve that the model is at best incomplete. The dotted line is the result of using the combined east-west/north-south current system. It is noted that the amplitude of the excursions is greatly reduced by the addition of the north-south current system. Lastly, the solid line is the result of removing the external current systems as explained earlier, as well as using the combination current system. The model is again slightly improved.

In summary we have shown that the predicted ionospheric current density distribution across the auroral oval is highly sensitive to the choice of model. In particular, for the example shown in Fig. 11b, we have shown that the best model includes both the north-south and east-west ionospheric currents (along with their associated field-aligned currents as per Boström (1964)), and that the effects of distant current distributions of significant intensity cannot be ignored in the evaluation of the model current density distribution across the auroral oval.

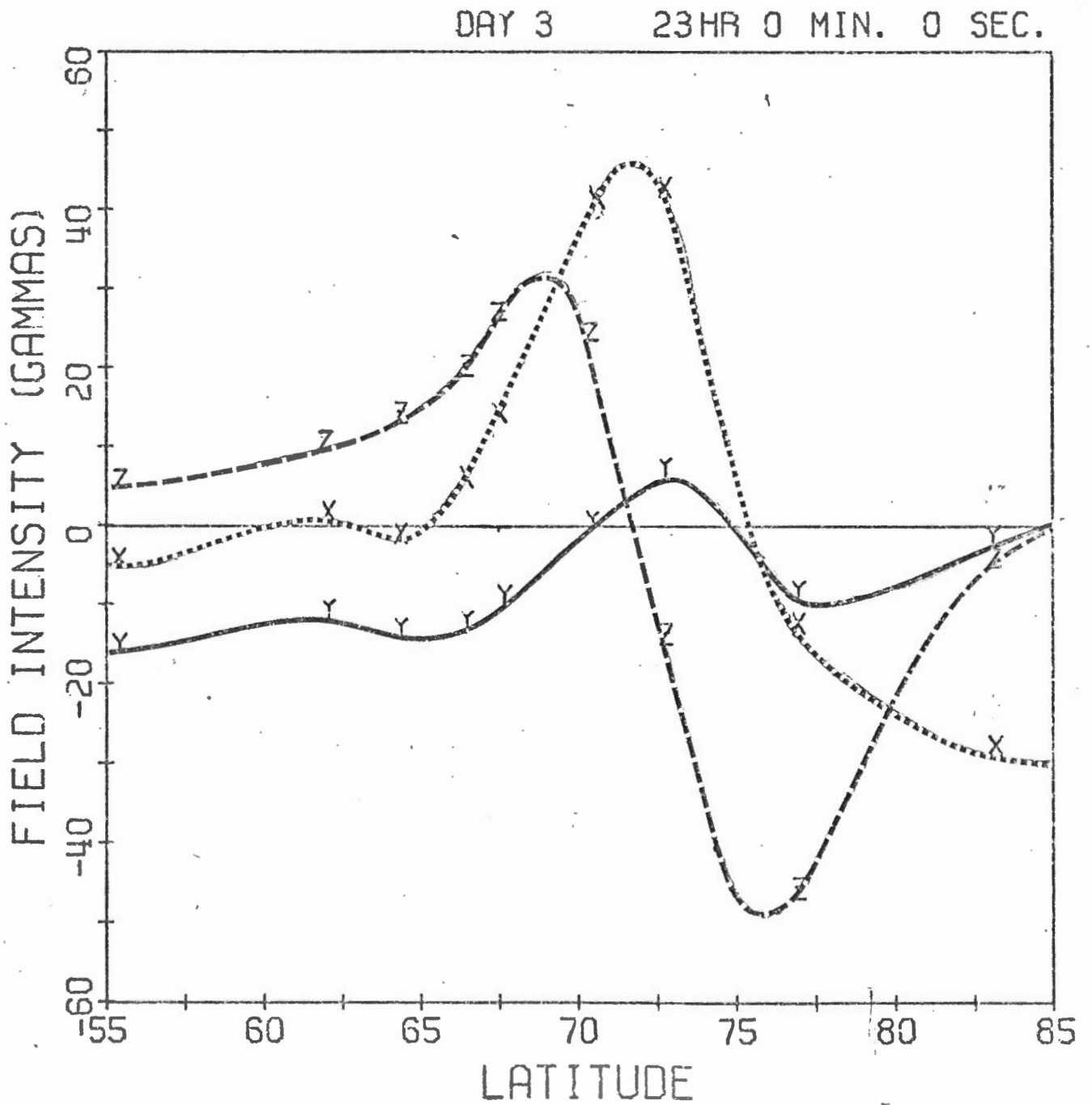
Figure 11a: A plot of the flattest model current distribution resulting from 3 inversions of the data shown in Figure 11b. (---) is the result when a simple three-dimensional east-west current system is used. (.....) is the result when the east-west system is combined with a three-dimensional north-south system. (—) is the result when the data is corrected for external current systems, and then modelled using a superposed east-west and north-south current system.

DAY 3; 2300 HOURS U.T.



LATITUDE (°)

Figure 11b: The averaged latitude profile for 2300 to 2400 UT day 3 of 1972. The results of inverting this data are shown in Figure 11a.



## Results

A typical set of averaging functions for real data is shown in Figures 13-15 and the latitude profile for which these functions were calculated is shown in Figure 12. The profile is indicative of both eastward and westward flowing current, lying between about  $62.5^{\circ}\text{N}$  and  $75^{\circ}\text{N}$  (i.e.  $27.5^{\circ}$  and  $15^{\circ}$  colatitude). The averaging function for a moderate value of the trade off parameter ( $\pi/4$ ) is shown for the northern ( $\theta = 15.00$ ) and southern ( $\theta = 27.50$ ) extrema, as well as for an intermediate colatitude ( $\theta = 20.00$ ). It should be noted in Figure 13 that the averaging function peaks at  $16.5^{\circ}$  colatitude, although this function was computed for  $\theta_0 = 15^{\circ}$ . This means that  $\langle J(\theta) \rangle$  for  $\theta = 15^{\circ}$  will be somewhat contaminated by values of  $J$  at higher colatitudes. This is not unusual for the data to be presented here, i.e. the estimate obtained by inversion for  $\langle J(\theta_0) \rangle$  for small  $\theta_0$  may be an average centered at some value of  $\theta$  slightly higher than the desired  $\theta_0$ . This is not a major problem in that the exact current bounds are impossible to determine in most cases, to within less than  $1-2^{\circ}$ , from the latitude profiles. Apart from this minor criticism, the curves of  $A(\theta, \theta_0)$  for real data are remarkably similar to theoretical curves and it is therefore expected that good estimates of  $\langle J \rangle$  will be obtained.

One example of a latitude profile and its inversion, chosen as typical for each hour between 1500 to 2200 MLT will be presented.

Figure 16 is a typical latitude profile for 1500 to 1600 MLT. In terms of a simple ionospheric current, this profile would be interpreted as primarily an eastward current lying between approximately  $66^{\circ}\text{N}$  and  $80^{\circ}\text{N}$ . The negative  $\Delta H$  north of  $75^{\circ}$  can be removed by assuming the presence of

Figure 12: Average latitude profile for day 17, 1972 for the interval 0600 to 0700 UT (2200 to 2300 MLT).

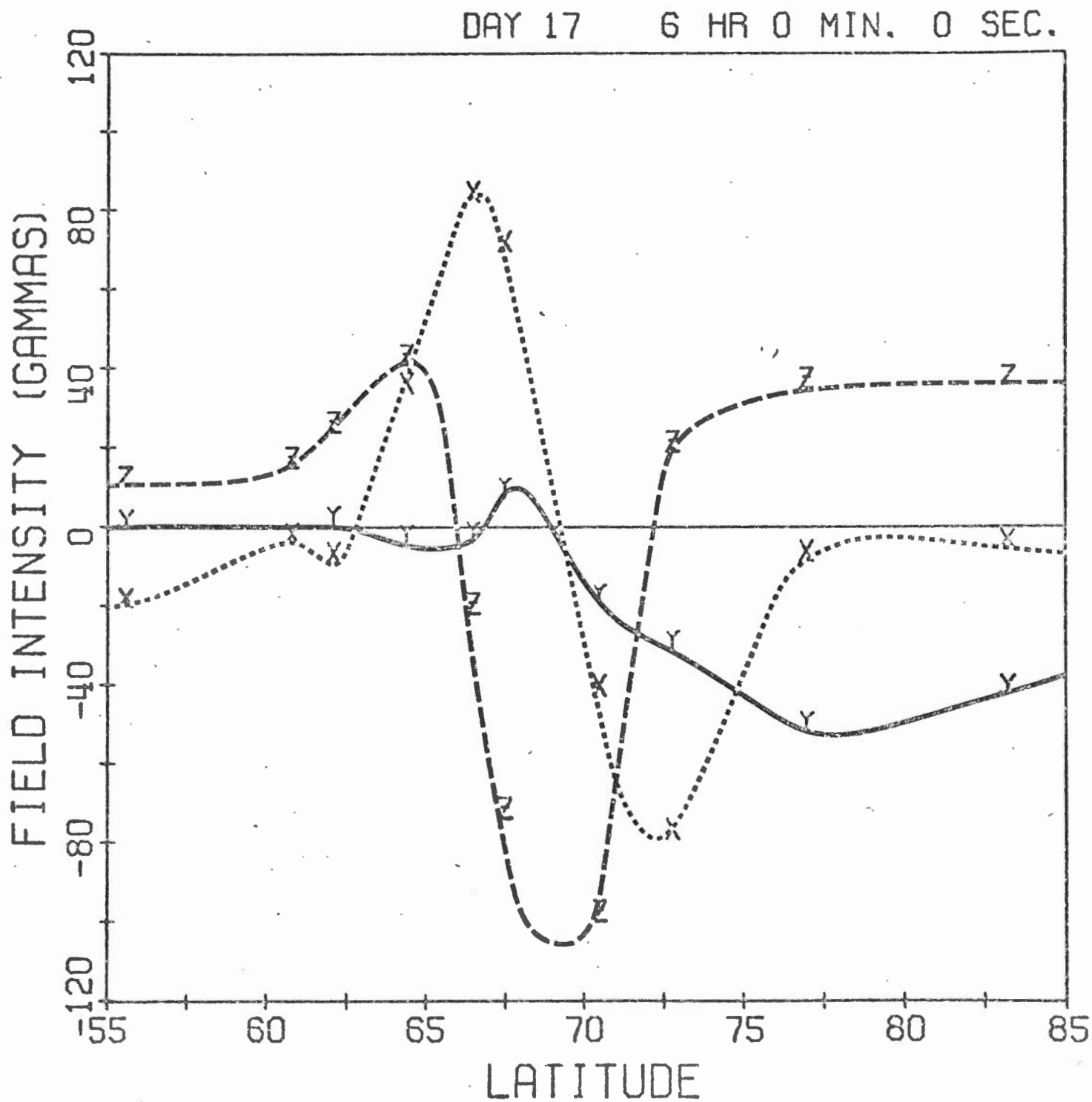


Figure 13: The averaging function  $A(\theta, \theta_0)$  for  $\theta_0 = 15^\circ$ , for the data shown in Figure 12.

THETA = 15.00      TRADE-OFF 0.7854

(X  $10^{-1}$ )

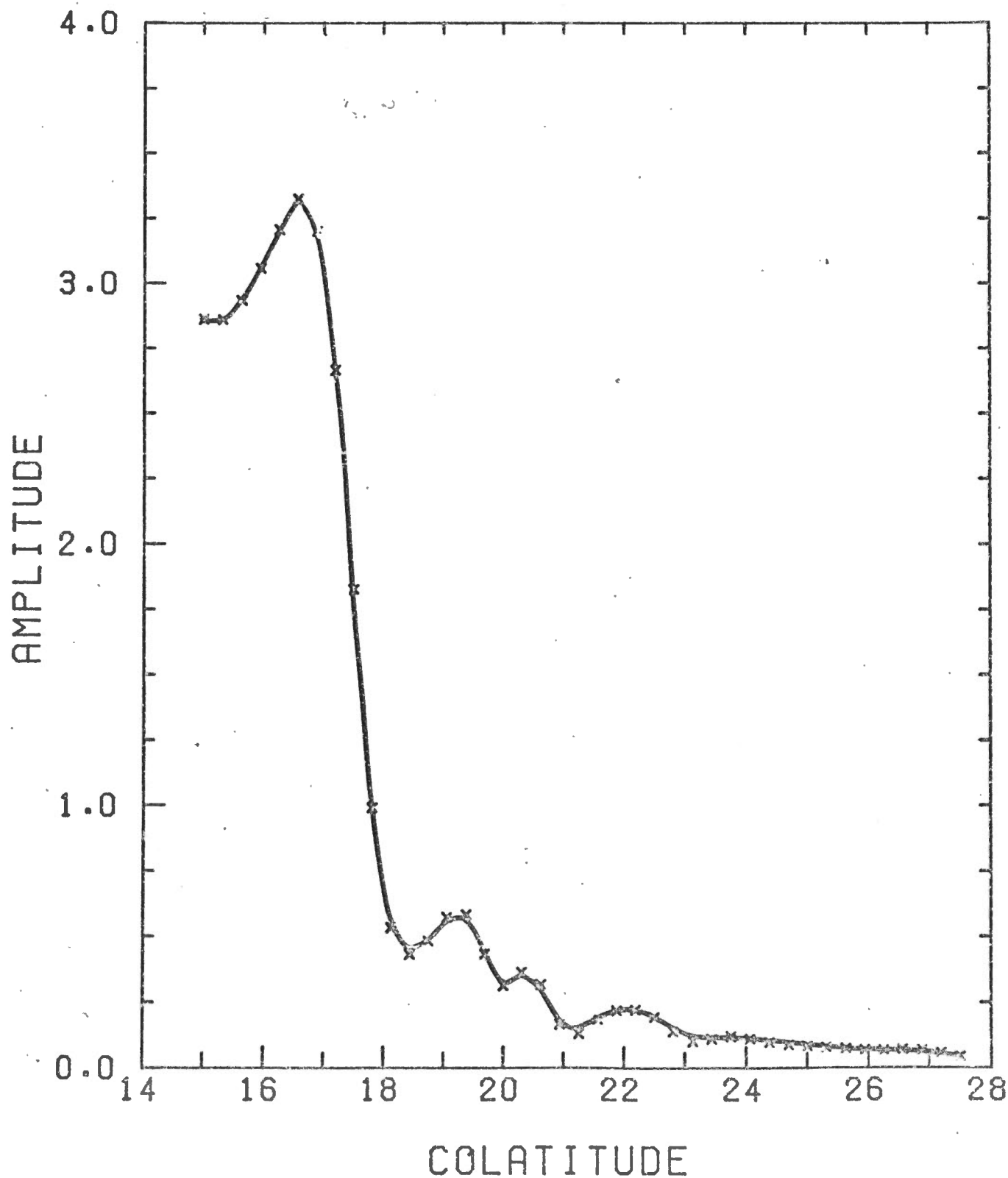


Figure 14: Same as Figure 13, for  $\theta_0 = 27.5^\circ$

THETA = 27.50      TRADE-OFF 0.7854

(X  $10^{-1}$ )

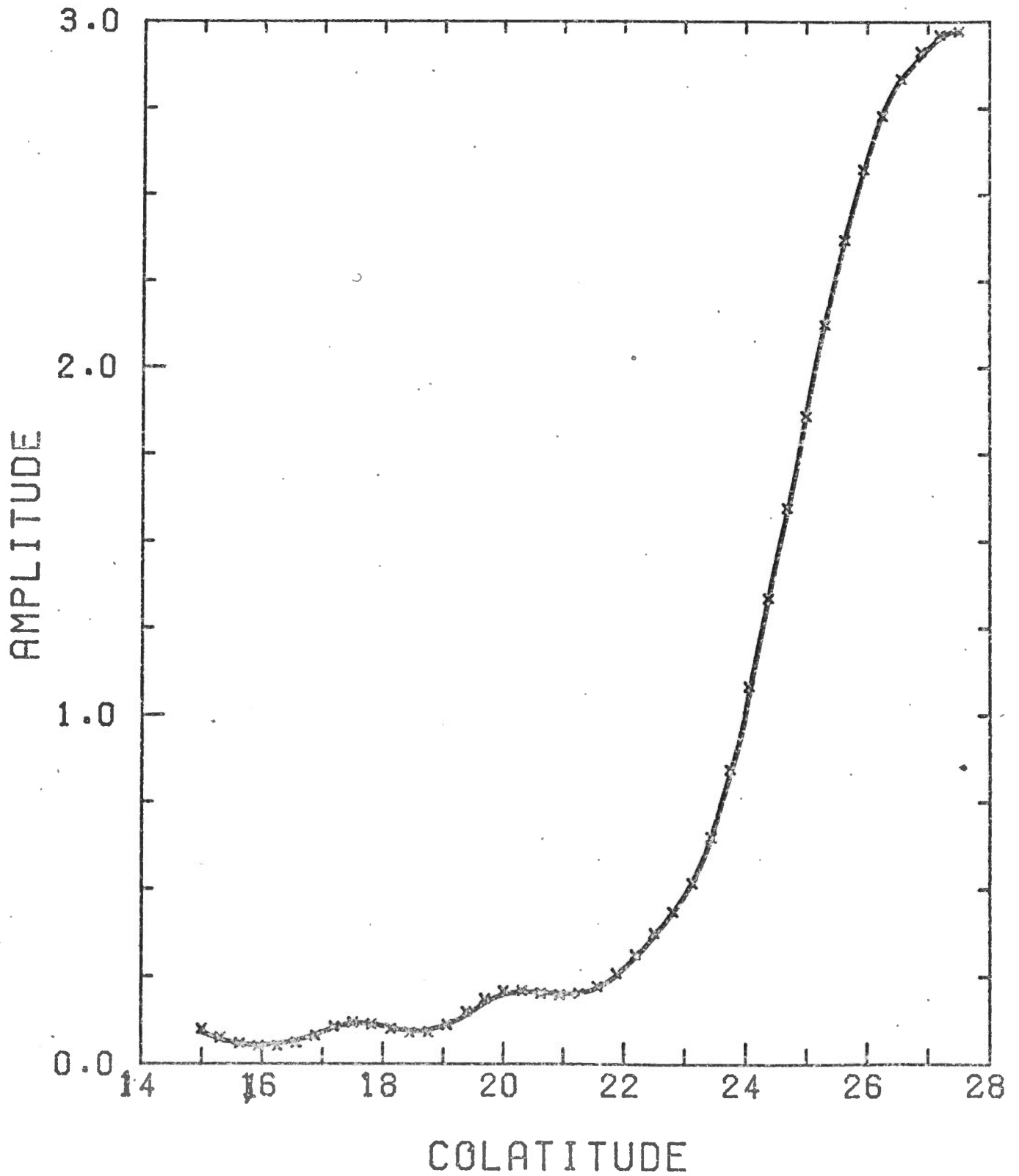


Figure 15: Same as Figure 13, for  $\theta_0 = 20^\circ$ .

THETA = 20.00      TRADE-OFF 0.7854

(X  $10^{-1}$ )

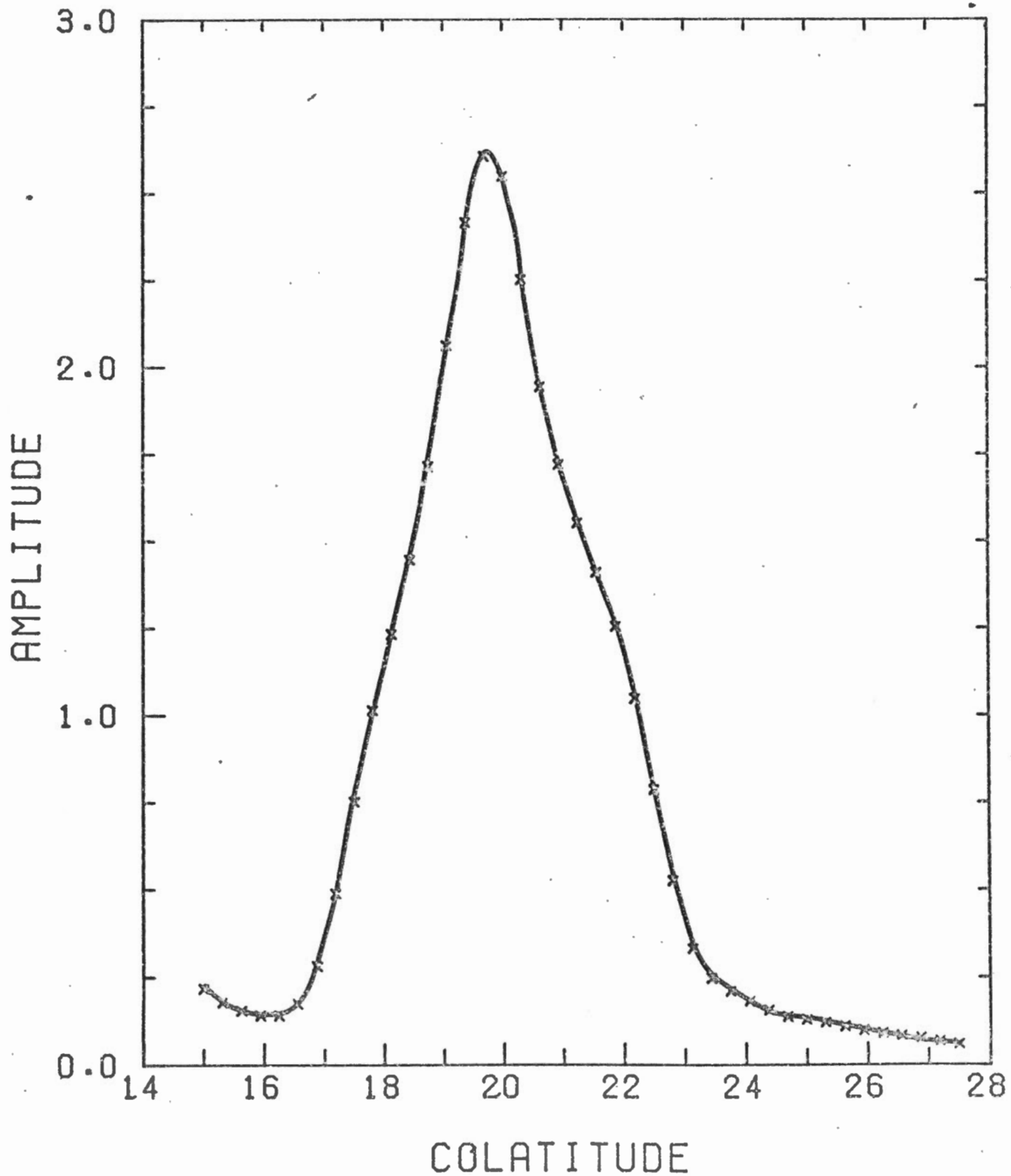
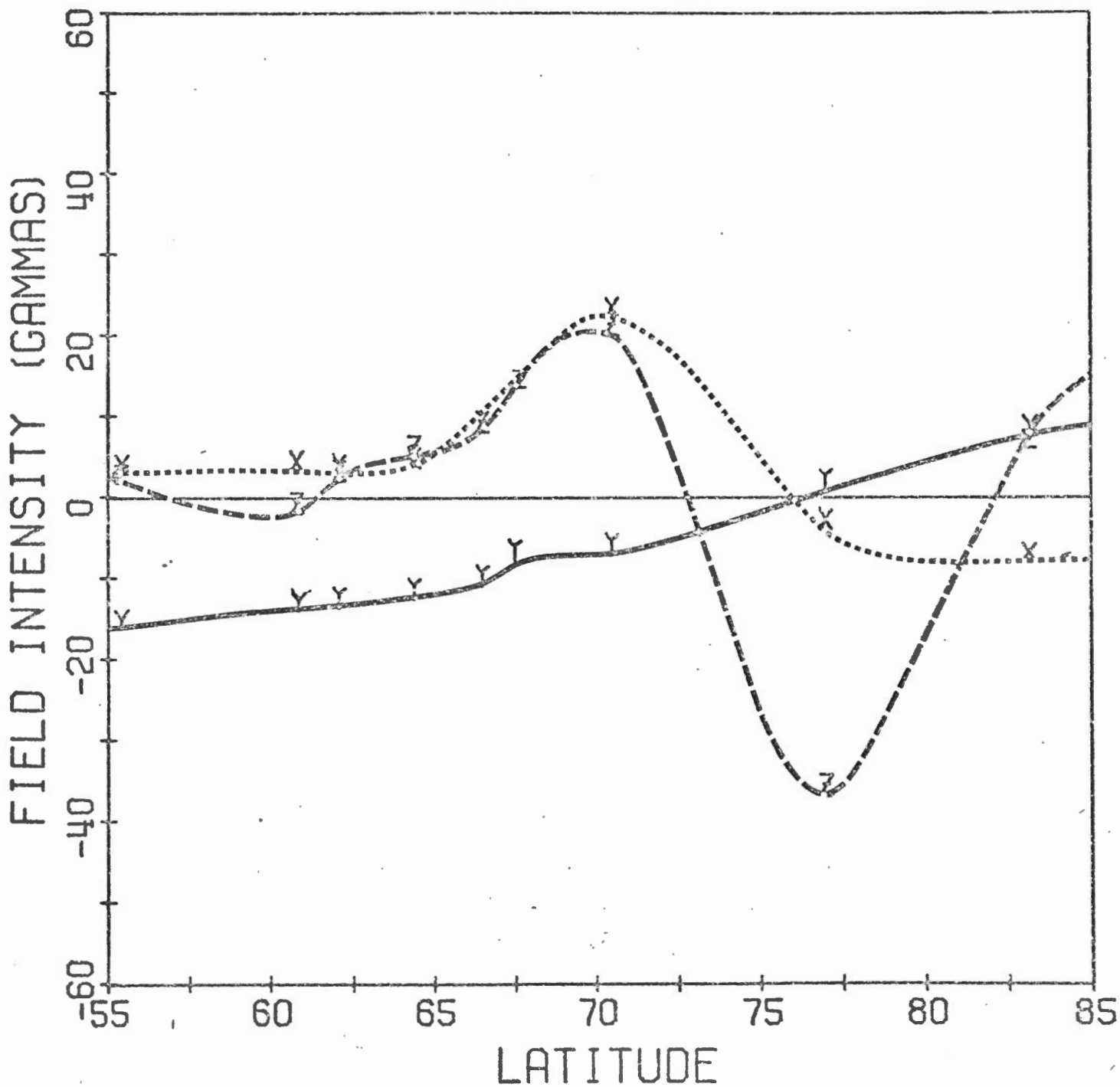


Figure 16: Average latitude profile for the hourly interval 2300-2400 UT (1500-1600 MLT) of day 13, 1972.

DAY 13 23HR 0 MIN. 0 SEC.



the three-dimensional current system involving poleward flowing Pedersen current as well as the other auroral current system across the pole in the morning sector. The result of inverting the H and Z component data (labeled X and Z in Figure 16 and subsequent latitude profiles) is shown in Figure 17. The solid line is the curve for  $\langle J(\theta) \rangle$  and the broken line is the plot of the flattest model. The current density estimates have been chosen from a set of estimates, one for each of several values of the trade-off parameter. Each point on this curve was picked on the basis of the width of the averaging function the error in the estimate as well as the form of the flattest model. Since the flattest model is only one of infinitely many models which can be generated to fit the data, it has been used only as a guide in deciding the form of the current density estimates. In this case,  $\langle J(\theta) \rangle$  is roughly parabolic, with a peak at about 0.006A/m. The total eastward current flowing in the electrojet is  $(6.7 \pm 0.5) \times 10^4$ A.

In interpreting the current density inferred from the flattest model, it is important to note that the positive peaks shown near co-latitudes of  $\sim 11.5^\circ$  and  $\sim 22^\circ$  should not be considered as evidence of real westward ionospheric current flow. This can be seen from the fact that there is no indication of westward current flow in the inverted data (solid curve). The positive peaks are, in fact, part of the oscillations associated with inaccuracies in the choice of all the current model parameters for the model system as well as for the external systems. Reduction of these oscillations to minimal amplitude would, in effect, produce the most correct model for the current configurations responsible for the magnetic variations shown in our latitude profile.

Figure 18 is a typical profile from the next one hour period,

Figure 17: The result of inverting the data shown in Figure 16.  
(---) flattest model current density curve. (—) estimates of current density  $\langle J(\theta) \rangle$ .

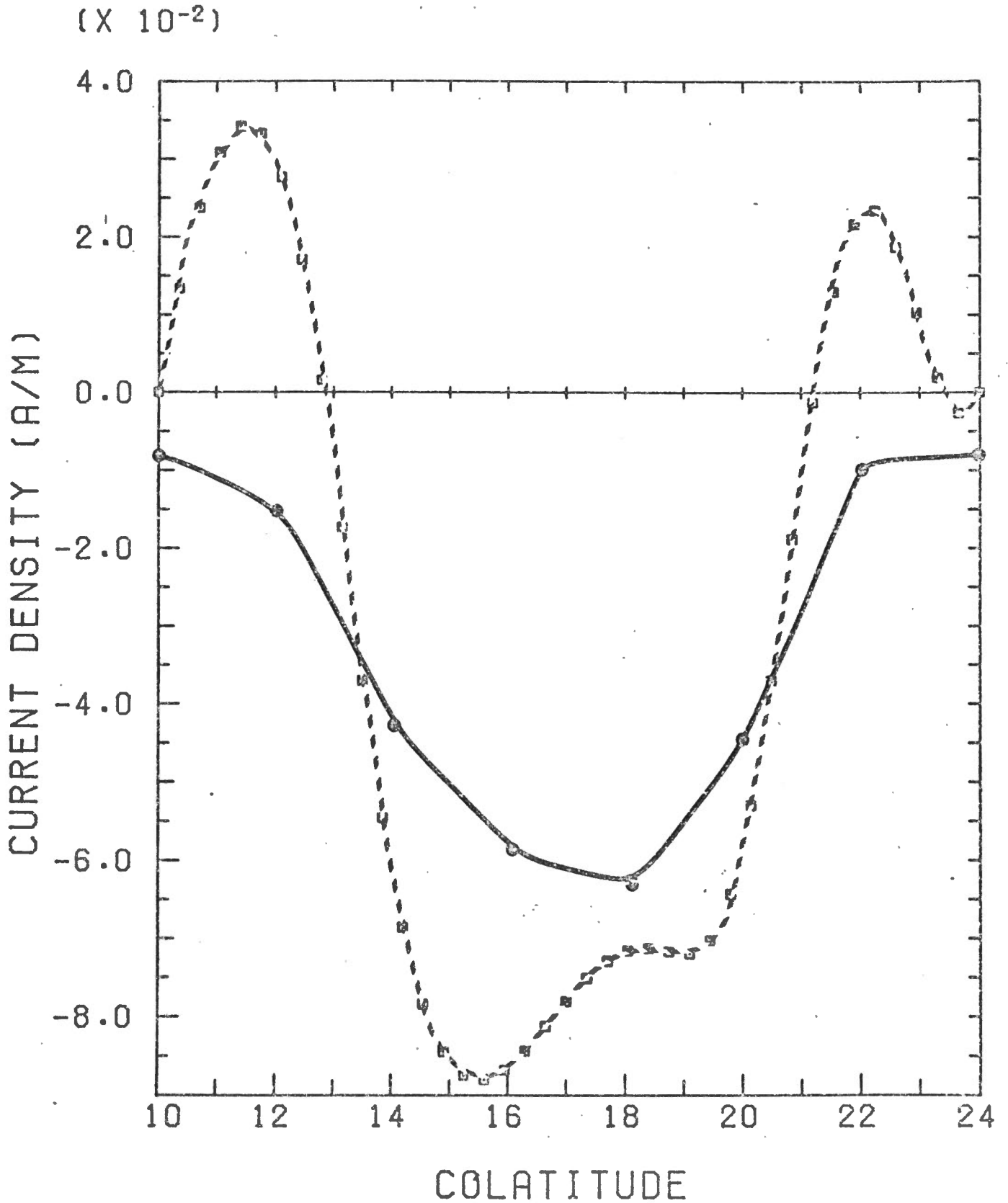
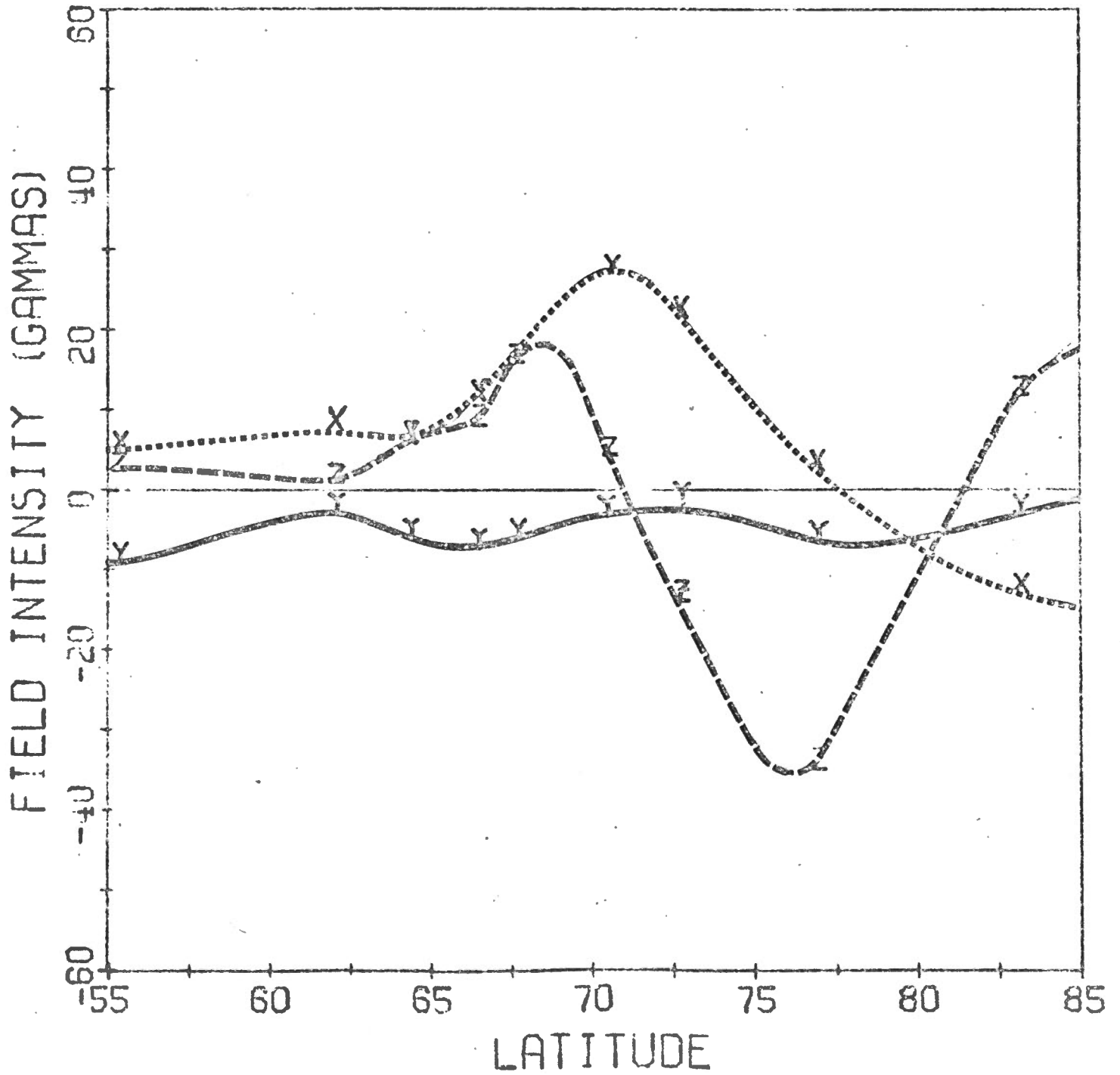


Figure 18: Average latitude profile for the hourly interval 0000-0100 UT (1600-1700 MLT) of day 3, 1972.

DAY 3 0 HR 0 MIN. 0 SEC.



1600-1700 MLT. This profile also indicates eastward flowing current lying between approximately  $67^{\circ}\text{N}$  and  $76^{\circ}\text{N}$ . Inversion of this data (Fig. 19) yields an oscillatory flattest model, but one in which the current flow is predominantly eastward. The current density estimates indicate a broad eastward current, approximately uniform across the width of the electrojet.

Figure 20 shows the final profile from the pre-dusk sector (1700-1800 MLT). The latitude profile is suggestive of purely eastward current along the auroral oval, and this is confirmed by both the inversion technique and by the flattest model (Figure 21). These results are consistent with those in the previous two hourly intervals, indicating the similar physical behaviour of the electrojet(s) across the auroral oval in the MLT interval 1500-1800.

To this point the, inversion of latitude profiles in the pre-dusk sector indicates only a broad eastward current as the average persistent feature. The character of the latitude profiles changes in the post-dusk sector. Figure 22 is typical of the profiles made for dusk to 1900 MLT. Interpretation of this profile in terms of a simple east-west current system would result in placing westward current between  $\sim 70^{\circ}\text{N}$  and  $76^{\circ}\text{N}$ , and a much weaker eastward current equatorward of this, extending to about  $63^{\circ}\text{N}$ . Inversion of this profile (Fig. 23) does not give a clear cut flattest model indicating that, there are errors in the model parameters. However, this is an average profile over a zone in which the nature of the current flow changes from pure eastward to mixed eastward and westward, and this is not taken into account in the model. The nature of the current distribution can be determined from the current density estimates  $\langle J(\theta) \rangle$ . The inversion results (solid curve) shown in Figure 23 indicate, then, that there is both

Figure 19: The inversion of the data shown in Figure 18.

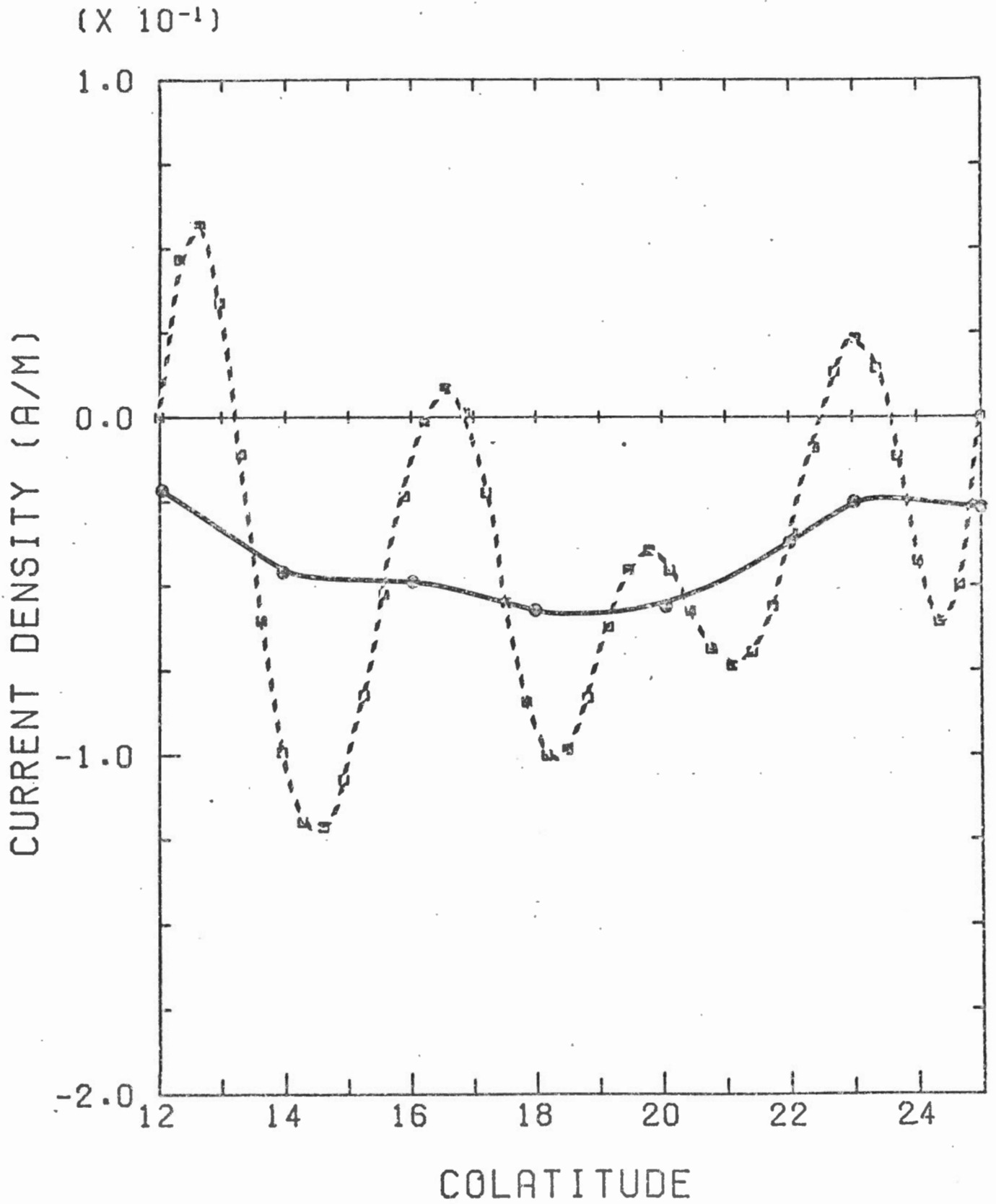


Figure 20: Average latitude profile for the hourly interval 0100-0200 UT (1700-1800 MLT) of day 15, 1972.

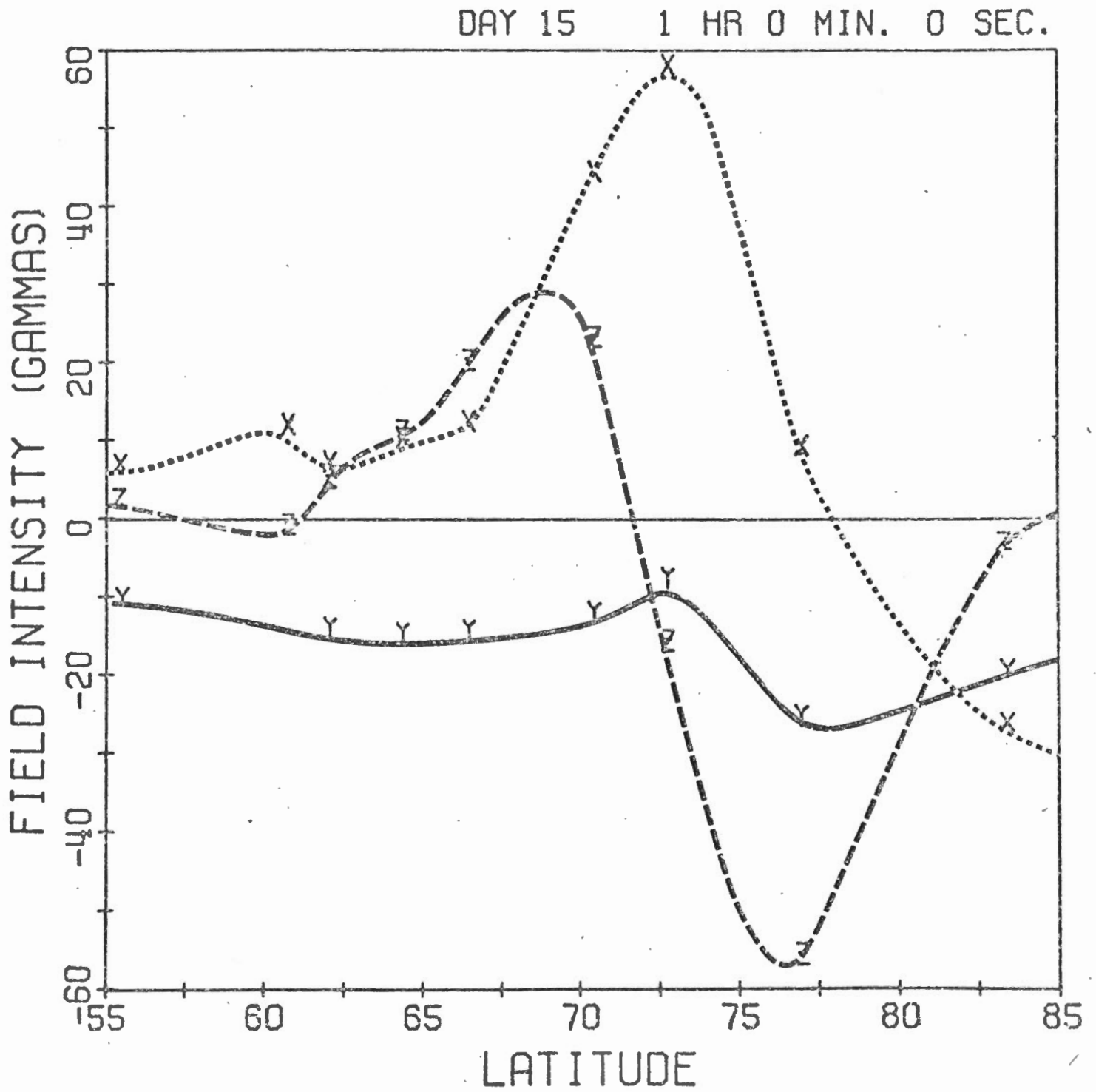


Figure 21: The inversion of the data shown in Figure 20.

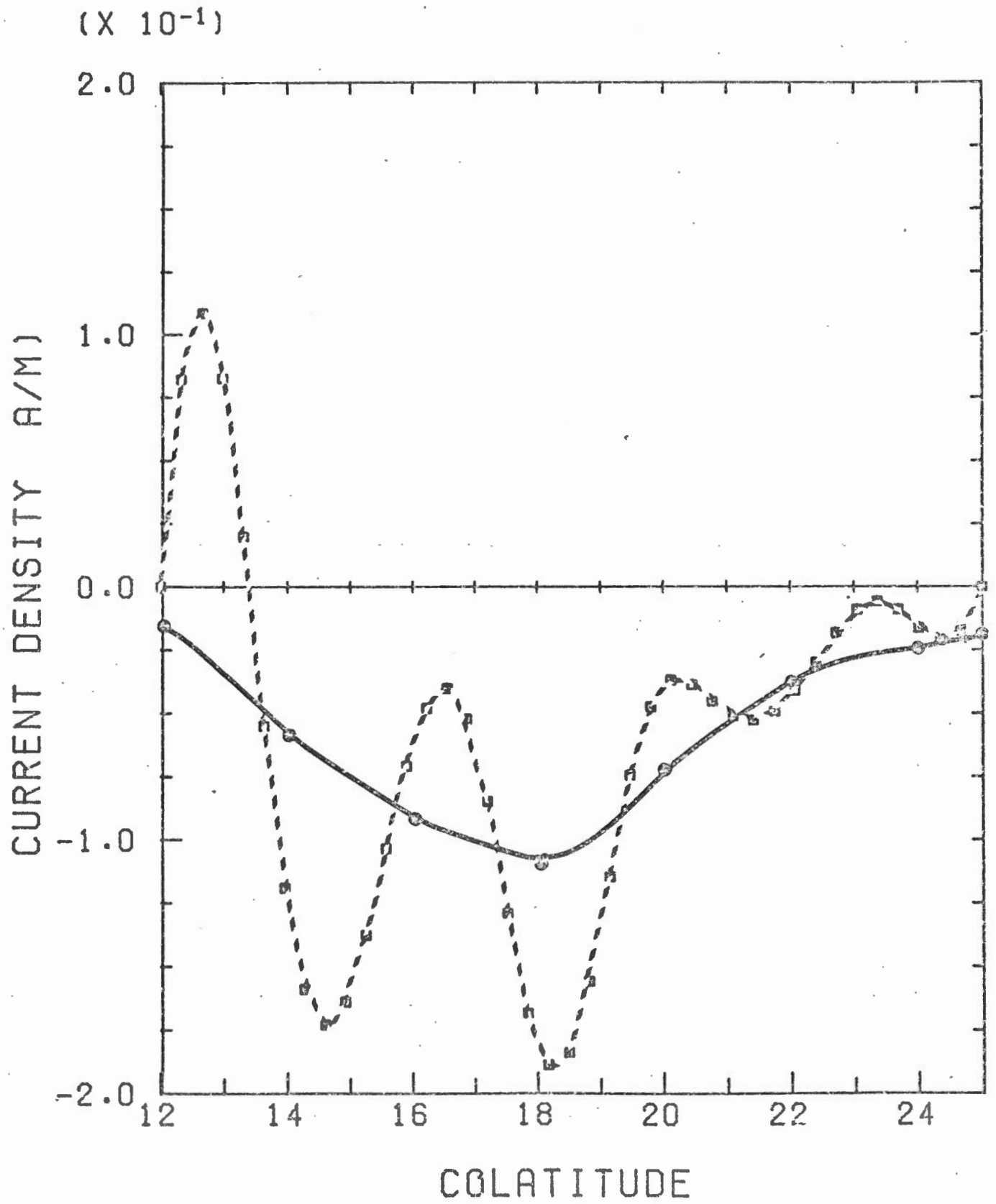


Figure 22: Average latitude profile for the hourly interval 0200-0300 UT (1800-1900 MLT) of day 333, 1971.

DAY 333 2 HR 0 MIN. 0 SEC.

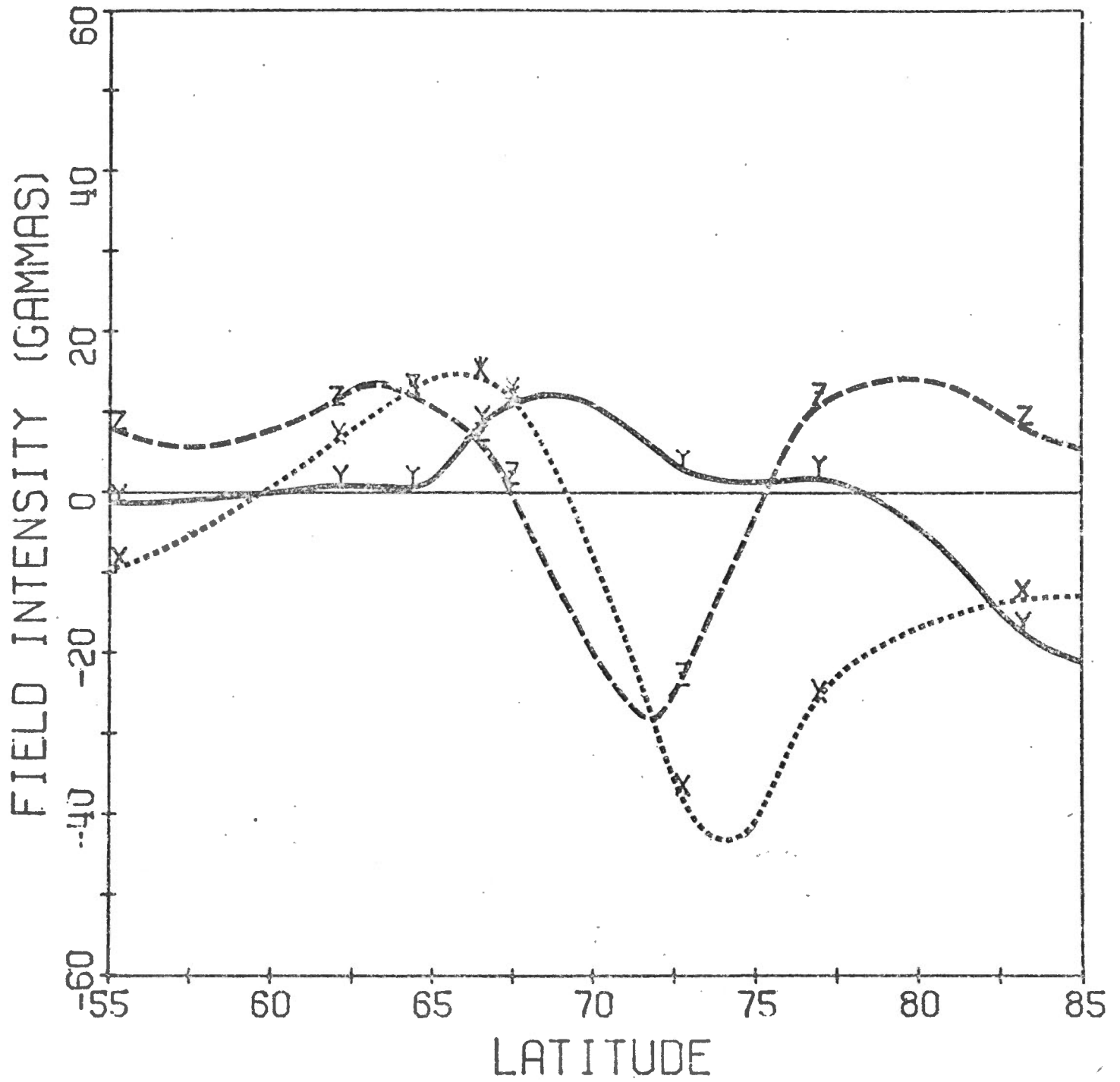


Figure 23: The inversion of the data shown in Figure 22.

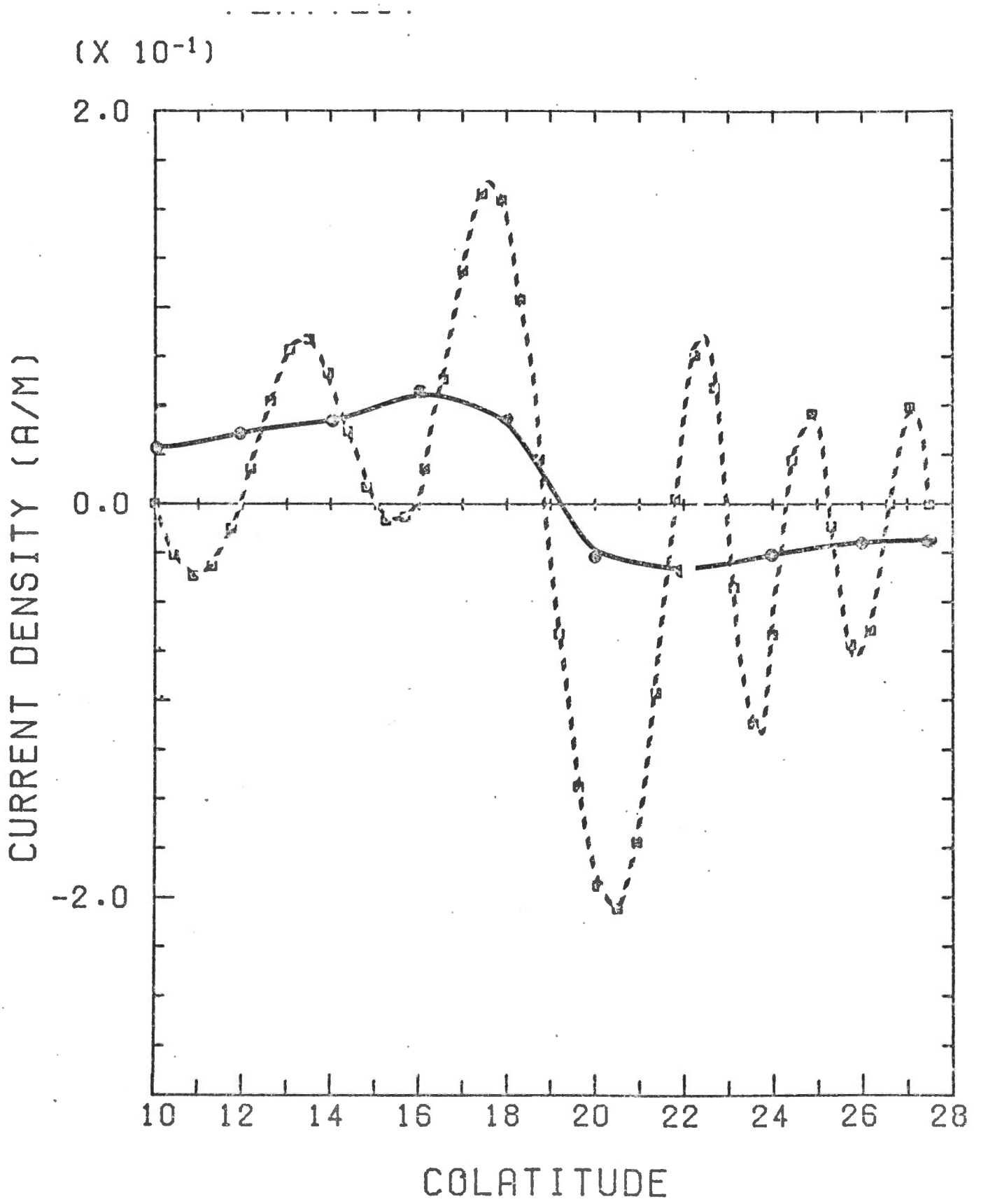


Figure 24: Average latitude profile for the hourly interval 0300-0400 UT (1900-2000 MLT) of day 18, 1972.

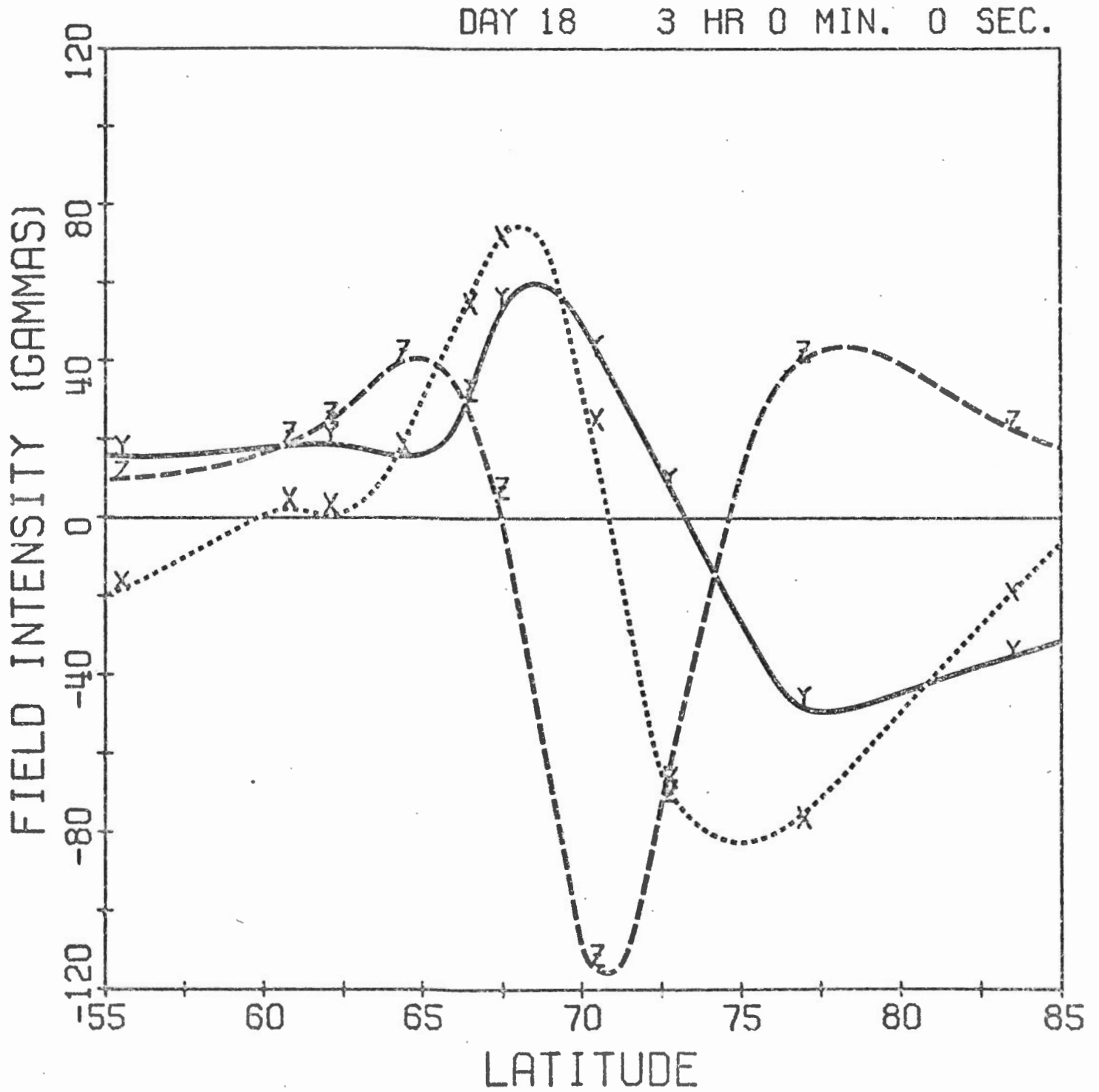


Figure 25: The inversion of the data shown in Figure 24.

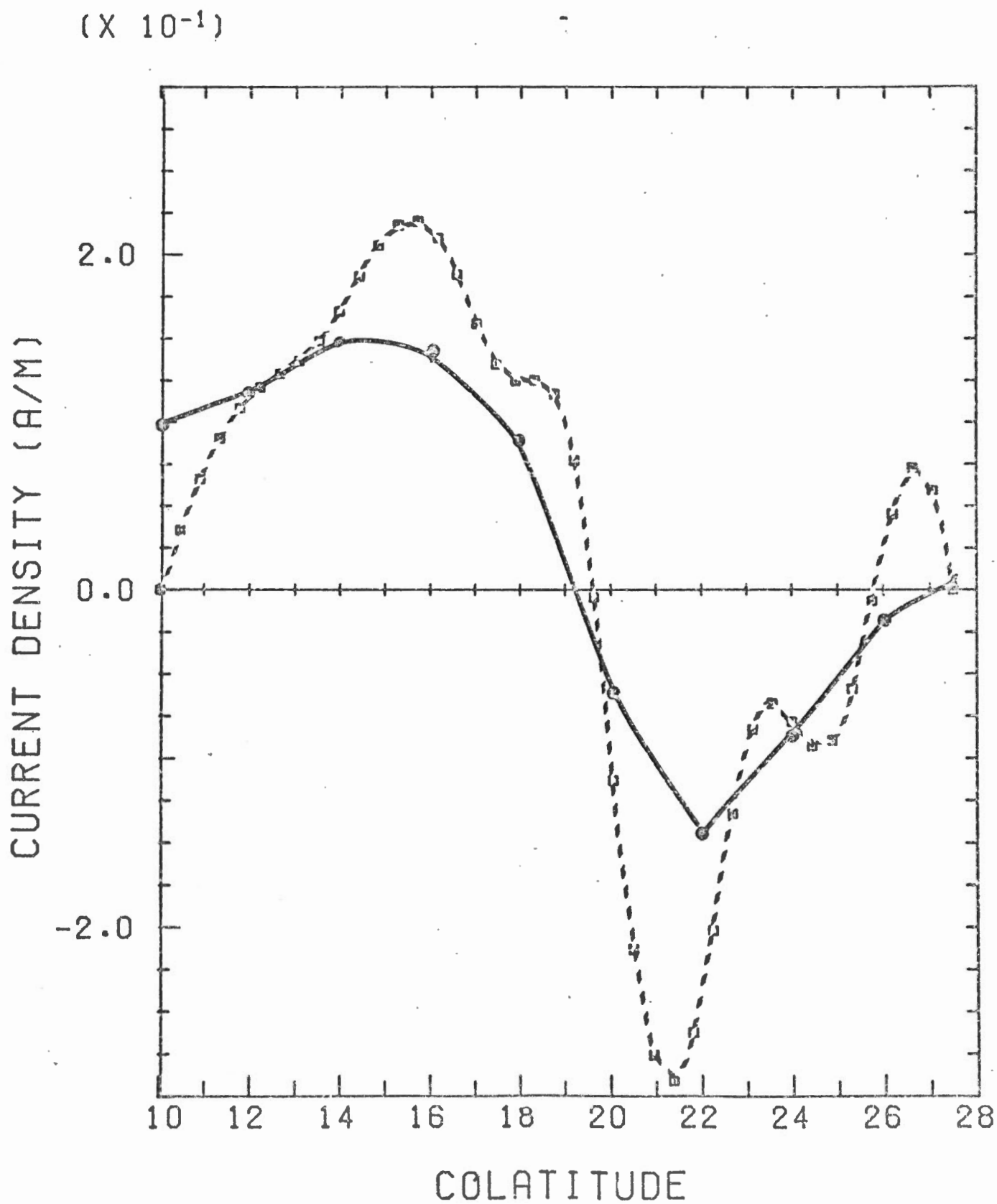


Figure 26: Average latitude profile for the hourly interval 0400-0500 UT (2000-2100 MLT) of day 338, 1971.

DAY 338 4 HR 0 MIN. 0 SEC.

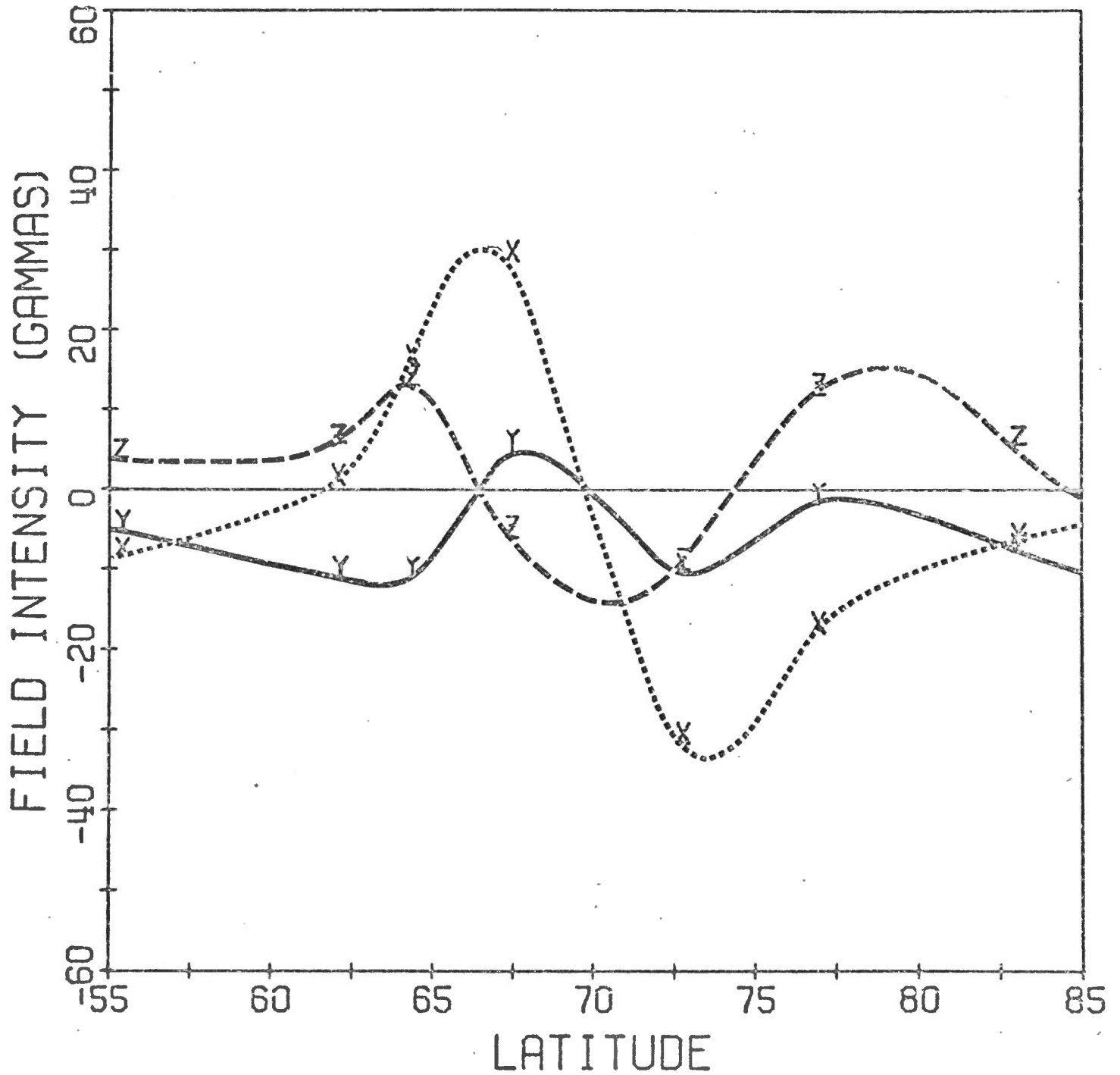


Figure 27: The inversion of the data shown in Figure 26.

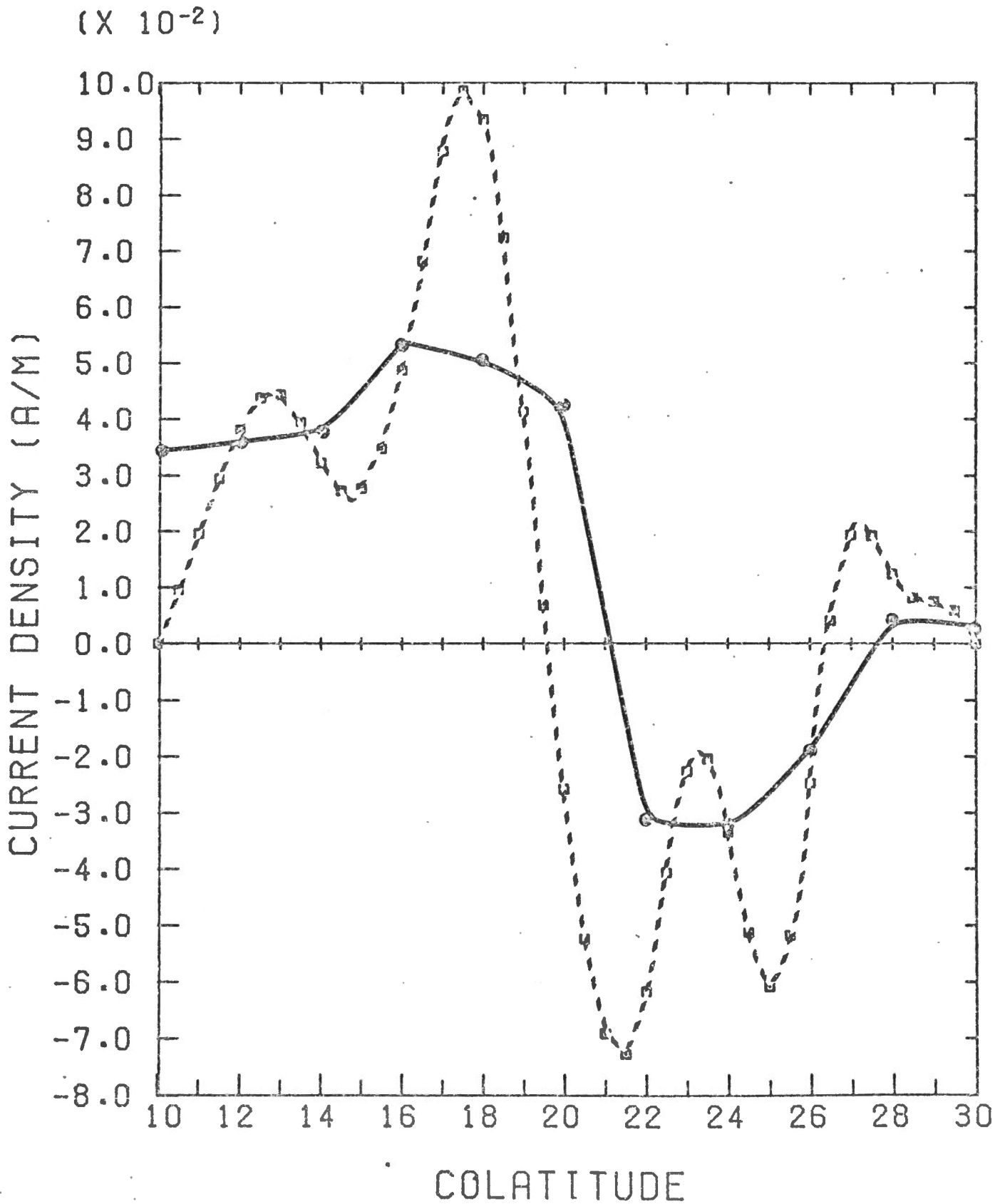


Figure 28: Average latitude profile for the hourly interval 0500-0600 UT (2100-2200 MLT) of day 335, 1971.

DAY 335 5 HR 0 MIN. 0 SEC.

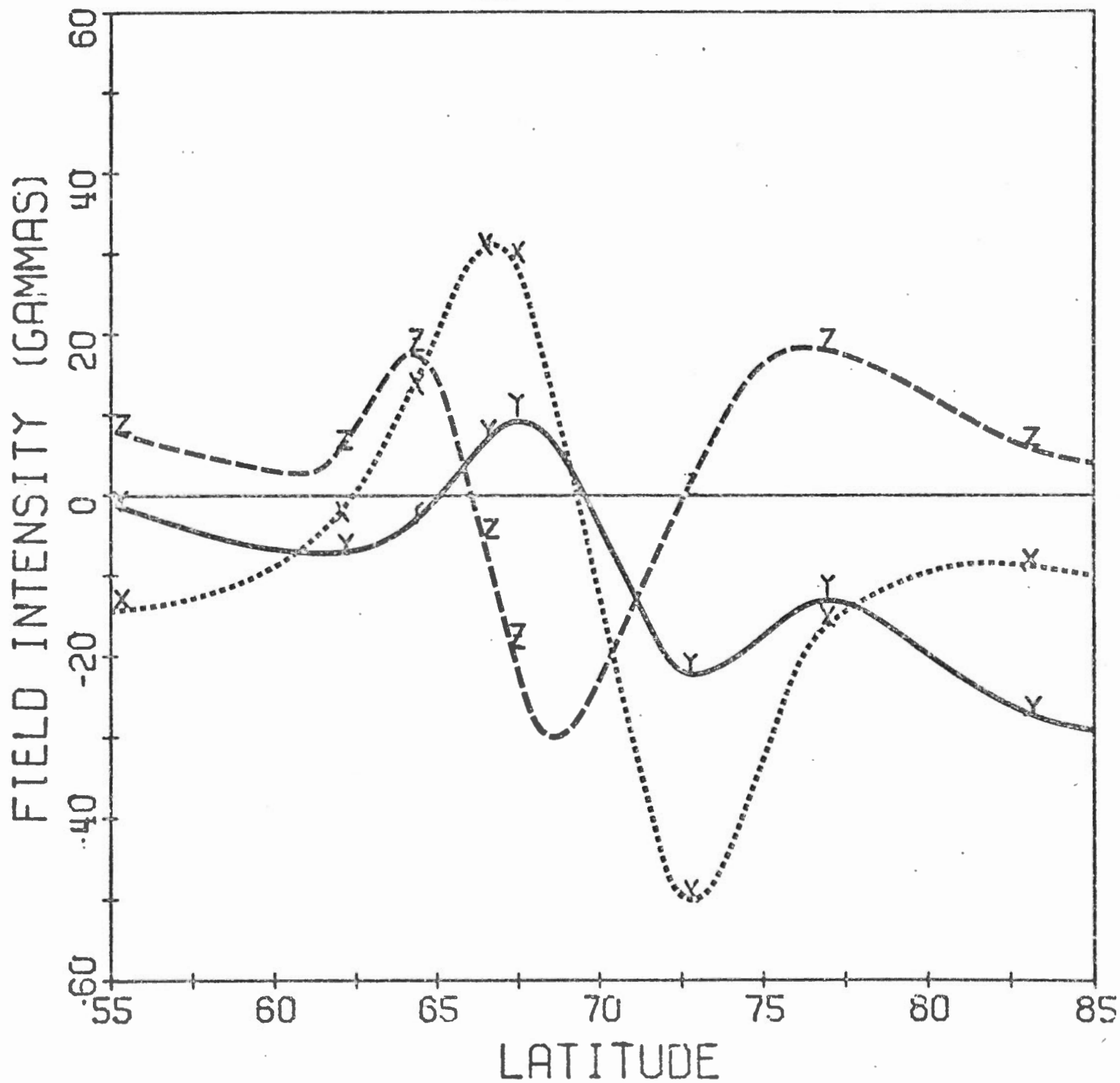


Figure 29: The inversion of the data shown in Figure 28.

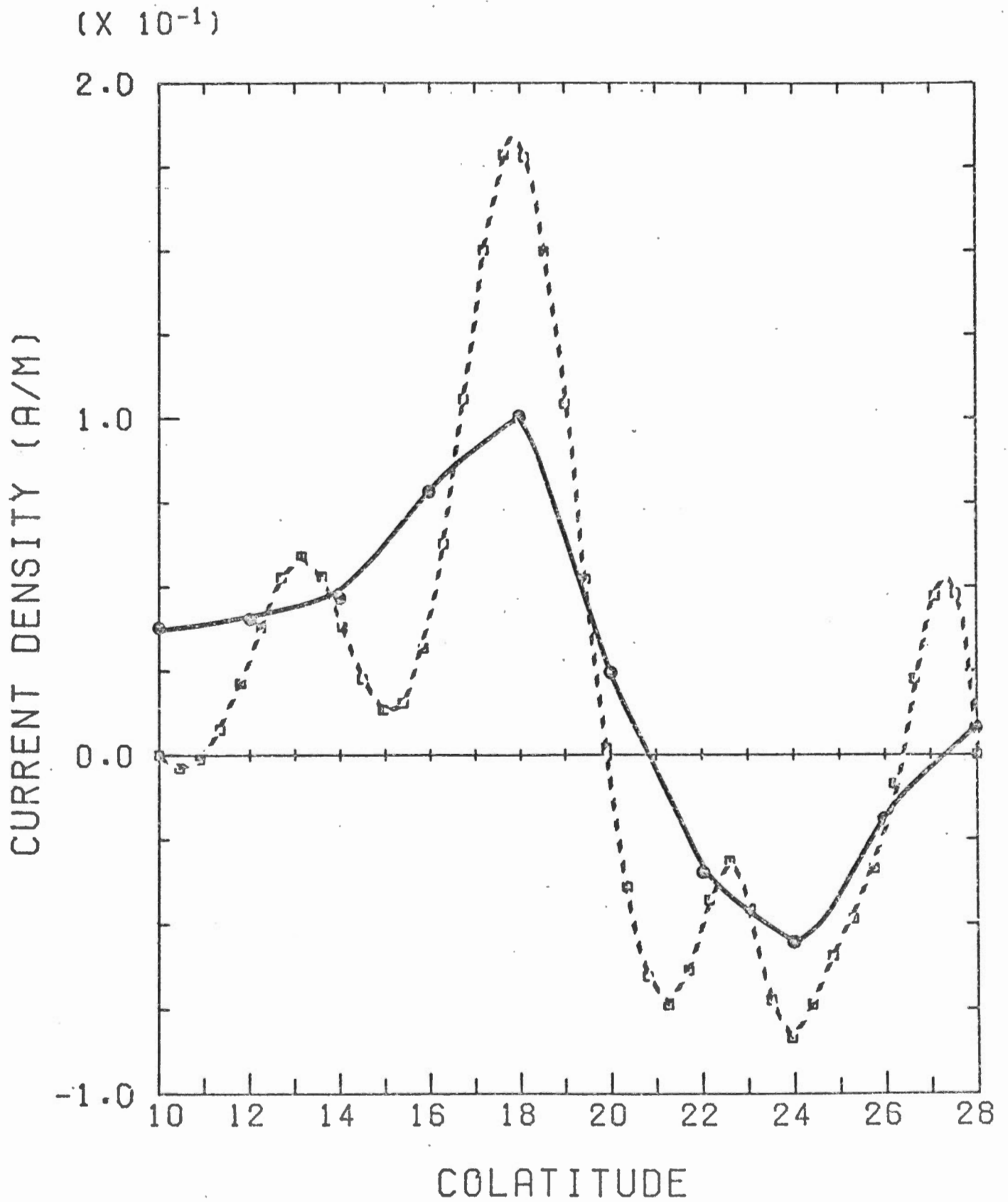


Figure 30: Inversion of the data shown in Figure 12, for the hourly interval of 0600-0700 UT (2200-2300 MLT) of day 17, 1972

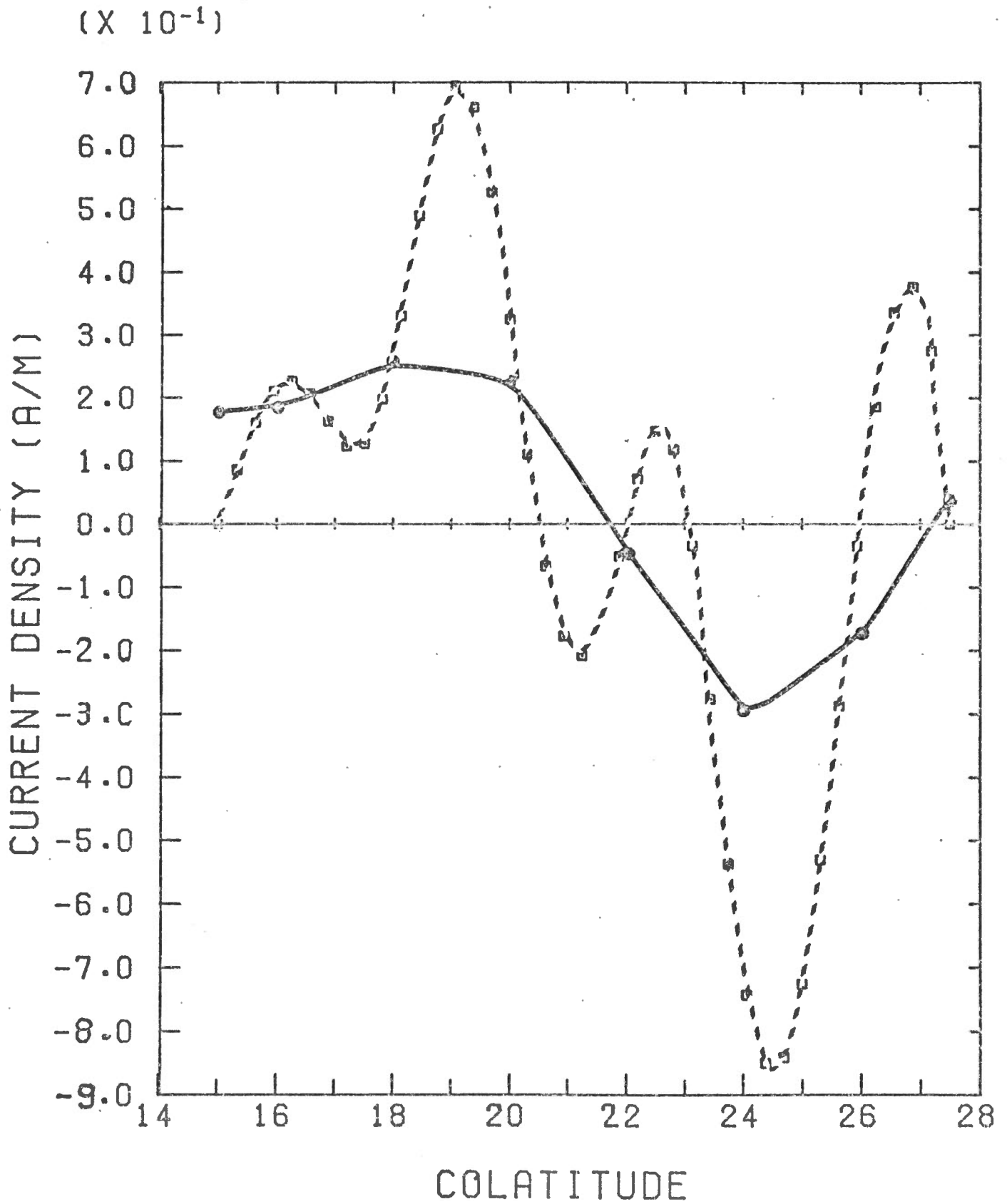
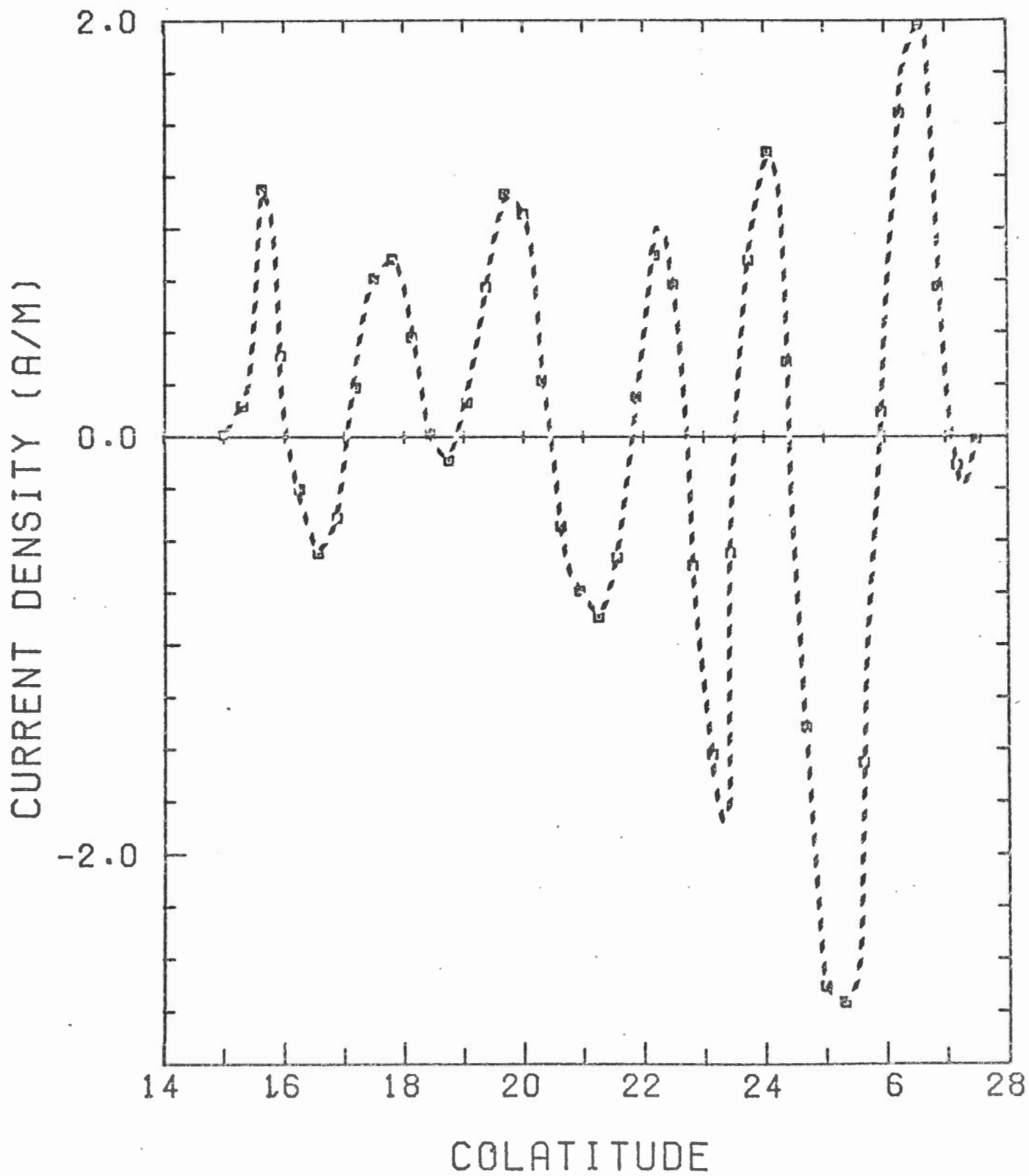


Figure 31: A plot of the "smallest" model current density for data from the hourly interval of 0600-0700 UT, day 17, 1972.



an eastward current (between about  $19^\circ$  and  $28^\circ$  colatitude) and a westward current poleward of this ( $10^\circ$  to  $19^\circ$  colatitude). The total current in the eastward jet is approximately 70% of that in the westward jet, a result which was not anticipated from the latitude profile.

All the average latitude profiles for the hours beginning at 1900 MLT to 2200 MLT indicate a double current system. Figure 24 is typical for 1900 to 2000 MLT. In this case, the flattest model is essentially unequivocal (Fig. 25) and the current density estimates indicate roughly parabolic current distributions. Similar results are obtained for 2000-2100 MLT (Figs. 26 and 27) and 2100-2200 (Fig. 28 and 29). Figure 30 is the result of inverting the data from the latitude profile shown in Figure 12. The flattest model in this case is less unambiguous with respect to the latitude at which the transition from westward current flow to eastward current flow occurs, than in the previous 3 hours; however, this time period is adjacent to the region of the Harang discontinuity and we might expect that we are approaching external current systems whose effects result in significant errors in our choice of the free parameters of the model. Applying corrections to the model to account for end effects of the currents flowing in the Harang discontinuity is difficult to carry out and this probably accounts for the poorer flattest model. The estimates  $\langle J(\theta) \rangle$  are unequivocal in indicating the presence of two anti-parallel current flows.

For completeness, one example of a "smallest" model (Equation 8) has been included. Although such models were routinely computed, it was found that they were of little help in determining the nature of the current density. Figure 31 is the smallest model that coincides with Figures 12

and 30. The current model in Figure 31 does fit the data, and this does serve to emphasize the non-uniqueness of this whole problem. However, it is of little other assistance.

### Discussion

The purpose of this study was to verify the existence of a westward current flow poleward of the eastward convection electrojet as a permanent feature of the magnetic local time sector between 1800 and 2300 hours. The results presented here are consistent with this. Although only one example of each hourly interval in this sector (and several hourly intervals prior to the dusk meridian) have been shown in this report several examples from each hour have been analyzed, and these all yield the same qualitative results. Prior to local magnetic dusk, only a broad eastward current flow is observed. From dusk to approximately 2300 MLT the latitude profiles and their inversions indicate that both a westward current and an eastward current coexist as a steady state feature. Although the magnitudes of these 2 currents vary from profile to profile, the shape of the current distribution curves are remarkably similar and it is tempting to correlate this with particle precipitation profiles and electric field profiles. In general, the current distributions are roughly parabolic, in agreement with Scrase's (1967) description of the auroral electrojets. Rostoker and Kisabeth (1973) have shown that eastward and westward electrojets exist simultaneously in this time sector during polar magnetic substorms. The fact that similar patterns of current flow exist both as a steady state feature and a disturbed feature is important to the understanding of magnetospheric processes, in that it would appear that

the substorm is a perturbation on a pre-existing current pattern. This observation may lead to further insight into the origin and driving mechanisms of polar magnetic substorms.

In summary the linear inverse theory of Backus and Gilbert (1970) has been applied to inversion of ground based magnetometer data to obtain latitudinal ionospheric current distributions (Oldenburg, 1976). This technique yields unique estimates of the current density as a function of colatitude. In order to facilitate interpretation of the results of this analysis, a model of current density which reproduces the data has been generated, i.e. the flattest model. It has been shown that this model produces an unrealistic current density if the current model parameters of the forward model are incorrect. It has been assumed therefore that if the flattest model of current density for real data is not smooth, then there are errors in the forward model free parameters, or alternatively, there are other current systems influencing the data. In the interpretation of the inversion results, several factors must be taken into account. Values of  $\langle J(\theta) \rangle$  are chosen in such a way as to use a narrow averaging function,  $A(\theta, \theta_0)$ , while yet minimizing the standard deviation of the estimates  $\langle J \rangle$ . In cases of doubt, reference has been made to the flattest model also. However, it must be emphasized that the flattest model is only one of an infinite set of models of current density that will reproduce the data. It is not necessarily a model of the real current density distribution. The spatial oscillations which appear in the flattest current density model have been assumed, in light of the discussion of the theoretical examples, to be only a reflection of the correctness of the forward current model.

References

- Alfvén, H. A theory of magnetic storms and of the aurorae, Kungl. Sv. Vetenskap. - Akad. Handl., III, 18(3), Stockholm, 1939.
- Armstrong, J. C. and A. J. Zmuda. Field-aligned current at 1000 km in the auroral region measured by satellite, J. Geophys. Res., 75, 7122, 1970.
- Armstrong, J. C., S.-I. Akasofu and G. Rostoker. A comparison of satellite observations of Birkeland currents with ground observations of visual aurora and ionospheric currents, J. Geophys. Res., 80, 575-586, 1975.
- Backus, G. and F. Gilbert. Uniqueness in the inversion of inaccurate gross Earth data, Phil. Trans. R. Soc., A266, 123, 1970.
- Birkeland, K. The Norwegian Aurora Polaris Expedition, 1902-03, Christiania, Vol. 1, Sect. 1, 1908.
- Birkeland, K. The Norwegian Aurora Polaris Expedition, 1902-03, Christiania, Vol. 1, Sect. 2, 1913.
- Boström, R. A model of the auroral electrojets, J. Geophys. Res., 69, 4983, 1964.
- Brekke, A., J. R. Doupnik and P. M. Banks. Incoherent scatter measurements of E-region conductivities in the auroral zone, J. Geophys. Res., 79, 3773, 1974.
- Fejer, J. The effects of energetic trapped particles on magnetospheric motions and ionospheric currents, Can. J. Phys., 39, 1409, 1961.
- Hughes, T. J. and G. Rostoker. Current flow in the magnetosphere and ionosphere during periods of moderate activity, J. Geophys. Res., 82, in press, 1977.
- Kamide, Y., S.-I. Akasofu and G. Rostoker. Field-aligned currents and the auroral electrojet in the morning sector, J. Geophys. Res., 81, 6141-6147, 1976.
- Iijima, T. and T. A. Potemra. The amplitude distribution of field-aligned currents at northern high latitudes observed by Triad, J. Geophys. Res., 81, 2165, 1976.
- Kern, J. W. A charge separation mechanism for the production of polar auroras and electrojets, J. Geophys. Res., 67, 2649, 1962.
- Kisabeth, J. L. and G. Rostoker. Modelling of three-dimensional current systems associated with magnetospheric substorms, Geophys. J., in press, 1977.

- Mozer, F. S. and P. Lucht. The average auroral zone electric field, *J. Geophys. Res.*, 79, 1001, 1974.
- Oldenburg, D. W. Ionospheric current structure as determined from ground based magnetometer data, *Geophys. J.*, 46, 41, 1976.
- Oldenburg, D. W. A quantitative technique for the modelling of ionospheric and magnetospheric current distributions, manuscript in preparation.
- Rostoker, G. Interpretation of magnetic field variations during substorm, *Earth's Magnetospheric Processes*, ed. by B. M. McCormac, D. Reidel Publ. Co., 379, 1972.
- Rostoker, G. and J. L. Kisabeth. Response of the polar electrojets in the evening sector to polar magnetic substorms, *J. Geophys. Res.*, 78, 5559, 1973.
- Scrase, F. J. The electric current associated with polar magnetic substorms, *J. Atmospheric Terrest. Phys.*, 20, 567, 1967.
- Sugiura, M. and T. A. Potemra. Net field-aligned currents observed by Triad, *J. Geophys. Res.*, 81, 2155, 1976.
- Wallis, D. D., C. D. Anger and G. Rostoker. The spatial relationship of the auroral electrojets and the visible aurora in the evening sector, *J. Geophys. Res.*, 81, 2857, 1976.
- Yasuhara, F., Y. Kamide and S.-I. Akasofu. Field-aligned and ionospheric currents, *Planet. Space Sci.*, 23, 1355, 1975.
- Zmuda, A. J., F. T. Heuring and J. H. Martin. Dayside magnetic disturbances at 1100 kilometers in the auroral oval, *J. Geophys. Res.*, 72, 1115, 1967.
- Zmuda, A. J., J. C. Armstrong and F. T. Heuring. Characteristics of transverse magnetic disturbances observed at 1100 km altitude in the auroral oval, *J. Geophys. Res.*, 75, 4757, 1970.
- Zmuda, A. J. and J. C. Armstrong. The diurnal flow of field-aligned currents, *J. Geophys. Res.*, 79, 4611, 1974.